FRONT MATTER

Title

- **Disrupted spatial and contextual memory encoding in the hippocampus of 5xFAD mice precedes cognitive impairment**

Authors

Yimei Li,[1] Mary Ann Go,[1] Hualong Zhang,[1,2] Simon R Schultz[1*]

Affiliations

1. Centre for Neurotechnology and Department of Bioengineering, Imperial College London, United Kingdom
2. Department of Biomedical Engineering, University of Melbourne

Abstract

Alzheimer's disease (AD) is marked by progressive cognitive decline, yet the underlying neural mechanisms are not fully understood. To address this, we investigated hippocampal activity in 5xFAD model mice performing a continuous spatial alternation task, combining behavioural assessment with *in vivo* two-photon calcium imaging. Young 5xFAD mice exhibited mild performance deficits, which worsened with age. Older 5xFAD mice showed significant impairments in task acquisition and alternation accuracy, with significant behavioural hyperactivity. Hippocampal CA1 neurons in 5xFAD mice showed early impairments in spatial representation, prior to showing behavioural deficits. Both young and old 5xFAD mice exhibited reduced spatial tuning, fewer place cells, and decreased trial-to-trial reliability in comparison to wildtype sibling controls. Additionally, 5xFAD mice demonstrated disrupted spatial encoding of reward locations, with reduced spatial correlation between correct and error trials. Analysis of hippocampal "splitter" cells revealed reduced splitting activity in 5xFAD mice, with reduced discriminability and reliability of trajectory-dependent activity. These deficits correlated with poorer task performance, suggesting that disrupted contextual encoding contributes to cognitive decline in AD. Our findings highlight early disruptions in hippocampal spatial and contextual encoding in 5xFAD mice, which precede behavioural impairments and provide insights into AD pathophysiology.

Teaser

Two-photon imaging in behaving AD mice reveals impairments in spatial and contextual memory circuits prior to cognitive deficits.

MAIN TEXT

Introduction

Alzheimer's disease (AD) is the most prevalent cause of dementia in older individuals, with a global prevalence particularly affecting those aged over 65 years (*1*). The amyloidogenic pathway generates amyloid-β (Aβ) and is implicated in other pathological features of AD, driving downstream pathophysiological signalling pathways that lead to neuronal death (*2-6*). Aβ accumulation is stable and largely completed prior to the onset of memory decline in patients with APP, PSEN1 or PSEN2 mutations (*7*). Remarkably, cognitive impairments may begin decades before the clinical diagnosis of AD dementia (*8*). Among cognitive impairments caused by the amyloidogenic pathway, spatial navigation deficits are particularly prominent, often detectable from the mild cognitive impairment stage (*9*). Furthermore, it has been reported that more than 60% of AD patients suffer from spatial memory deficits and wandering behaviours (*10*). These deficits are closely linked to hippocampal dysfunction. The hippocampus, a critical component of the medial temporal lobe memory circuit, is essential for forming and retrieving spatial and episodic memory. In AD, hippocampal CA1 neuronal morphology, plasticity, and neurogenesis are disrupted by Aβ and other pathological processes from early stages, as evidenced in both AD patients and mouse models (*11-13*).

Hippocampal place cells are essential for supporting spatial navigation and memory formation, yet they are degraded in AD. This degradation has been observed in various AD mouse models, including those with APP mutations and APP knock-in mice. For example, Tg2576 and hAPP mice exhibit degraded hippocampal place fields and reduced spatial information, which correlates with the onset of behavioural cognitive deficits (*14, 15*). In 3xTg AD mice, hippocampal neurons show a reduction in spatial information and a decreased proportion of place cells that phase-lock to theta and slow gamma rhythms prior to detectable Aβ accumulation (*16, 17*). In 5xFAD mice, weakened synaptic efficacy and a reduction in sharp wave-ripples (SWRs) during place cell reactivation have been reported (*18*). Moreover, environmental remapping of hippocampal place and grid cells is severely impaired in APP knock-in mice, with disruption of context discrimination (*19*). These findings collectively suggest that disrupted firing of hippocampal place cells destabilises spatial representations, contributing to the memory deficits in AD mouse models.

Unlike place cells, which primarily encode spatial locations, splitter cells represent contextual information linked to memory and task demands. Splitter cells were first identified by Wood et al. and Frank et al., who recorded hippocampal neuronal activity in rats navigating a continuous T-maze alternation task (*20, 21*). However, their role in AD remains poorly understood. The integrated computations of spatial and contextual coding during goal-directed, memory-guided navigation displayed by splitter cells suggest their potential as targets for investigating the mechanisms of cognitive impairments in AD.

Previous studies indicate that synaptic changes induced by Aβ may trigger dysfunction of hippocampal learning and memory in AD mouse models. In 5xFAD mice, basal synaptic transmission and long-term potentiation (LTP) at hippocampal Schaffer collateral-CA1 synapses are reduced by 6 months of age, coinciding with impaired contextual fear conditioning memory (*22-24*). In APP/PS1 mice, while fear memory formation and short-term memory (STM) remain normal at 7 months of age, dendritic spine density in hippocampal engram cells is reduced (*25*). However, it remains unclear whether the

degradation of hippocampal spatial and contextual representations occurs before or is coincident with the onset of cognitive behavioural impairments in AD models.

Addressing these questions is crucial for a deeper understanding of AD pathophysiology. We utilized the 5xFAD mouse model, which carries five familial Alzheimer's disease mutations associated with the APP and PSEN1 genes, and rapidly develops severe amyloid pathology. Previous studies have shown that intraneuronal Aβ42 is present from 1.5 months of age, with extracellular Aβ deposition beginning around 2 months (*23, 26*). Aβ levels and amyloid burden increase dramatically between 4 and 6 months of ages (*23*). Deficits in learning and memory appear from 4 months in 5xFAD mice (*27*). Based on these findings, we defined in our study a "young" AD group as mice younger than 4 months, and an "old" AD group as those older than 7 months of age. To assess spatial working memory, we introduced a novel behavioural paradigm in which head-fixed 5xFAD mice performed a continuous T-maze alternation task, which is sensitive to hippocampal dysfunction (*28, 29*). This paradigm was combined with two-photon calcium imaging to investigate hippocampal network activity. This approach enabled the simultaneous recording of activity from large populations of neurons at the single-cell level, providing a detailed view of how AD pathology affects hippocampal spatial representation and function. By focusing on the integrated computations of contextual and spatial coding during goal-directed navigation, this study highlights hippocampal splitting activity as an important target for probing the mechanisms underlying cognitive impairments in AD. Ultimately, the findings made here deepen our understanding of AD pathophysiology and may inform the development of more effective interventions.

Results

1. Head-fixed mice are able to acquire the continuous spatial alternation task in a real-world maze

We developed a novel behavioural paradigm to assess spatial memory in head-fixed mice, in which they performed a continuous spatial alternation task within a real-world, air-lifted maze setup. Our approach integrates the use of two-photon calcium imaging to capture the activity of populations of individual hippocampal neurons with high resolution during spatial navigation and memory tasks (Figure 1A, left). To motivate mice to navigate and learn the behavioural task, they were subjected to water restriction prior to the first day of training. In each trial, the mouse navigates from the location of the previous reward to a new reward location (the opposite side arm) through a common pathway (Fig. 1A, right). Mice are rewarded with 4 μl of liquid reward only when they choose the arm opposite to the one visited in the previous trial. The mice were trained 's trajectories are recorded, and both correct and error trials are tracked across up to 10 days of training (Fig. 1B). Behavioural performance is measured by the alternation percentage, which directly reflects learning and memory capabilities. Head-fixed mice were trained for 45 minutes each session twice a day. Task acquisition was defined as achieving an alternation percentage of 70% or higher in three consecutive sessions or over two consecutive days.

Over the course of training, we observed a significant improvement in alternation percentage (Fig. 1C, $F_{(9, 99)} = 11.58$, $P < 0.0001$), and a significant increase in the total number of trials achieved per day (Fig. 1D, $F_{(9, 99)} = 8.93$, $P < 0.0001$), indicating successful learning of the task in young healthy mice. Head-fixed mice typically reached the

performance criterion around day 7, maintaining stable alternation performance through to day 10. On error trials, mice exhibited higher running speeds in the side arm compared to correct trials, while speed remained similar in the central arm (Fig. 1E). This speed pattern suggests that the mice effectively recognized task-related movements, rather than engaging in random or gambled running behaviour.

2. 5xFAD behavioural performance are age-progressively impaired in the continuous spatial alternation task

After confirming that young, healthy mice could master the head-fixed alternation task within 10 days, we evaluated four groups of mice categorized by age and genotype: young (2–4 months) and old (7–12 months) mice, with genotypes defined as control (5xFAD−/−) and AD model (5xFAD+/−) mice.

All groups except the old 5xFAD mice demonstrated significant improvements in alternation performance over the training period (Fig. 2A). Except for the old 5xFAD group ($F_{(9,65)} = 0.65$, $P = 0.75$), all animals made significant improvements over the course of training. Young control mice demonstrated substantial accuracy improvement ($F_{(9,99)} = 11.58$, $p = 7.0 \times 10^{-12}$), as did old control mice ($F_{(9,59)} = 6.48$, $p = 4.7 \times 10^{-6}$) and young 5xFAD mice ($F_{(9,77)} = 2.81$, $p = 0.007$). Old control mice exhibited significantly lower alternation percentages than young control mice throughout the training. While the alternation performance of young 5xFAD mice was lower than that of young controls, the difference was not statistically significant. However, old 5xFAD mice showed a significant decline in performance compared to both old control mice and young 5xFAD mice. (group comparison: young 5xFAD vs young Ctrl, $F_{(1,158)} = 2.748$, $P = 0.0993$; old 5xFAD vs old Ctrl, $F_{(1,106)} = 5.271$, $P = 0.02$; young Ctrl vs old Ctrl, $F_{(1,149)} = 12.31$, $P < 0.0001$; young AD vs old AD, $F_{(1,124)} = 12.95$, $P = 0.0005$.). The task acquisition fraction further highlighted these differences, with old 5xFAD mice exhibiting the lowest proportion successfully acquiring the task during the training period (Figure 2B). Within the 10-day training window, 8 out of 10 young control mice successfully met the acquisition criteria. In contrast, 5 out of 8 young 5xFAD mice and 3 out of 6 old control mice met the criteria. The old 5xFAD group showed the most substantial reduction, with only 2 out of 7 mice achieving task acquisition.

Previous studies have reported hyperactive behaviours in both AD patients and mouse models of AD (*30, 31*), thus one might possibly expect AD mice to perform many trials, but with low accuracy. Consistent with this, we observed an age-dependent increase in the total number of trials completed within a 45-minute session in 5xFAD mice over the training period (Figure 2C). This increase in the number of total trials was accompanied by an elevation in running speed and reduced trials latency during the task, indicating that 5xFAD mice exhibit behavioural hyperactivity (Supplementary Fig. 1A, C). These findings further suggest that the reduced alternation percentages in old 5xFAD mice were not due to a lack of environmental exploration. In contrast, old control mice exhibited reduced total trial numbers and locomotion compared to young control mice (Fig. 2C, Supplementary Fig. 1A). The decreased movement observed in old control mice, in contrast to the hyperactivity seen in old 5xFAD mice, may be a factor contributing to the age-related decline in alternation performance in wildtype mice.

3. 5xFAD mice show spatial representations impairments prior to cognitive performance deficits

To investigate whether hippocampal CA1 neurons in 5xFAD mice show impaired spatial representations during the continuous spatial alternation task, we employed *in vivo* two-photon calcium imaging to record the activity of jGCaMP7s-expressing hippocampal CA1 neurons while mice performed a figure-8 task (Fig. 2D). To analyze neural calcium activity in conjunction with mouse trajectories, calcium transient trains from each neuron were aligned with the corresponding behavioural trajectory time points. The figure-8 maze was discretized into 1 cm-wide bins, forming a 32 x 32 grid, to construct spatial rate maps. For each bin, the spatial rate was calculated by dividing the sum of deconvolved calcium transient event amplitudes by the total time the mouse spent in that bin. Only running speeds greater than 8 mm/s were included in the spatial rate map calculation. A Gaussian kernel with a sigma value of [3, 3] bins was applied to smooth the spatial rate maps.

Although spatial tuning of neural activity was observed in both control and 5xFAD mice (Fig. 2E), the proportion of place cells was significantly lower in 5xFAD mice compared to controls (Fig. 2F: Young Ctrl 56±3% *vs* Young AD 45±4%, $P < 0.05$; Old Ctrl 39±4% *vs* Old AD 27±4%, $P < 0.05$). Additionally, 5xFAD mice exhibited significant age-related reductions in spatial information compared to healthy controls (Fig. 2G, Supplementary table 1). These results indicate that 5xFAD mice show impaired spatial tuning in neural activity prior to cognitive behavioural performance deficits during the alternation task. Furthermore, we found that correlation between running speed and population average hippocampal CA1 calcium activity was disrupted in 5xFAD mice (Supplementary Fig. 2), suggesting that speed-tuning of neural activity is also impaired in 5xFAD mice during the head-fixed alternation task.

4. 5xFAD mice show reduced trial-trial spatial tuning stability

To evaluate the stability of spatial tuning in CA1 neurons of 5xFAD mice within each imaging session, we analyzed the fraction of trials in which place cells remained active during the alternation task training. This analysis was further stratified into linearized figure-8 trials. Both young and aged 5xFAD mice showed a reduced proportion of trials exhibiting spatially tuning activity (Fig. 3A, B. Supplementary table 1), suggesting that fewer trials in 5xFAD mice retain consistent place cell activity, even at young ages. The trial-to-trial spatial correlations show stabilization of the spatial code within the imaging session. We next examined trial-to-trial correlation by calculating Spearman correlation coefficients between corresponding spatial activity bins on adjacent trials within the same imaging session. Our results revealed that CA1 place cells in 5xFAD mice exhibited a progressive age-related decline in trial-to-trial spatial reliability (Fig. 3C, D. Supplementary table 1) indicating impairments in the stability of spatial representations within training sessions in 5xFAD mice. This reduction is consistent with the decline in the proportion of place cells and spatial information, as 5xFAD mice exhibited trial-to-trial instability prior to alternation performance deficits.

5. Consistent session-to-session spatial tuning field in 5xFAD mice

The long-term stability of place cells supports hippocampal long-term memory (*32, 33*). We next examined whether the session-to-session spatial tuning activity across alternation behavioural training is degraded in 5xFAD mice. To assess the stability of place cells across

training stages, we imaged the same FOVs across 3 training stages: early (day 6), middle (day 8) and final (day 11). We then tracked the same populations of neurons across the 3 stages (Fig. 4A). We selected place cells that maintained significant spatial tuning activity across all 3 training stages (Fig. 4B).

First, we observed that some place cells demonstrated persistent and stable place field firing across all imaging stages, even in old 5xFAD mice (Fig. 4C, D). 5xFAD mice showed reduced the proportion of stable place cells but not significant when compared to the same age controls (Supplementary table 1). There was a only notable decrease in the proportion of stable significant place cells in old 5xFAD mice compared to young control mice (Fig. 4E, F, $P = 0.005$). To further examine whether the spatial selectivity of those stable place cells was altered in 5xFAD mice, we quantified the session-to-session correlation of place cells across training stages. Interestingly, both young and aged 5xFAD mice exhibited session-to-session correlations comparable to those of control mice (Fig. 4G, AD effect: $P = 0.1$; Age effect: $P = 0.3$). Moreover, the place field shifts in persistent place cells of 5xFAD mice did not show significant changes (Fig. 4H, AD effect: $P = 0.9$; Age effect: $P = 0.2$), indicating their ability to maintain stable spatial selectivity and place fields throughout the training. Taken together, these findings suggest that place cells in 5xFAD mice, compared to control mice, retain the normal stability to preserve consistent place fields across alternation task training. This may indicate that 5xFAD mice are still able to maintain subsets of place cells for stable spatial representations in a familiar environment. This result contrasts with trial-to-trial stability, which was greatly impaired in 5xFAD mice, suggesting that reactivations of spatial representations during the spatial alternation task are more vulnerable in the short-term than in the long-term.

6. 5xFAD place cells show reduced spatially tuned activity in the reward arm

Accurate representation of reward locations is crucial in the goal-directed task. Given the reward-driven nature of our alternation task, we examined how place cells respond to reward locations during both correct and error trials. Trials were categorized based on turn direction and reward location: correct left turns (RL), correct right turns (LR), error left turns (LL), and error right turns (RR). Mice were not rewarded during error trials (RR and LL). For each trial type, trajectories overlapped in the reward arms (Fig. 5A, B).

To examine spatial coding along reward arms, we analyzed the activity of cells which had place fields along the reward arm, and compared their spatial tuning activity during rewarded correct trials (RL and LR, Fig. 5C, left) and unrewarded error trials (LL and RR, Fig. 5D, left). Place cells located along the reward arm showed increased activity near the reward spout position in both trial types, with a noticeable decline after the reward spout. In 5xFAD mice, the peak spatial tuning activity of place cells along reward arms was significant reduced both in correct and error trials (Fig. 5C, D-right; Supplementary table 1).

Next, we further investigated whether 5xFAD hippocampal neurons are able to accurately encode the reward spout location during rewarded trials. The peak activity location in old 5xFAD mice was significantly shifted away from the reward spout, towards the post-reward arm (Fig. 5E, $Chi = 42$, $P < 0.0001$). Finally, we examined the spatial correlation of place cells between correct and error trials. 5xFAD mice exhibited an age-dependent reduction in correlation compared to control mice, suggesting a diminished ability to consistently encode

reward positions across trial types (Fig. 5F, G; AD × Age effect: $F_{(1,7335)} = 19.58$, $P < 0.0001$; YoungCtrl vs YoungAD: $P < 0.0001$; OldCtrl vs Old AD: $P = 0.01$). However, this reduction was not observed in place cells that have place fields in the return arms (Supplementary Fig. 3C). These findings suggest that the impairment encoding for reward locations in 5xFAD mice is not only related to the encoding of spatial information, but also to the encoding of reward-contextual information. Taken together, young 5xFAD mice exhibited reduced spatial encoding activity but still retain encode the accuracy of reward spout locations, which exhibited greatly shifts in old 5xFAD.

7. Hippocampal CA1 splitting activity degraded in 5xFAD mice

A splitter cell is a type of neuron whose tuning of activity on a common path (here the central arm) depends on a subsequent (or alternatively historical) choice made by the animal. Unlike place cells, which primarily encode spatial locations, splitter cells are thought to represent contextual information linked to memory and task demands. These cells reflect an internally organized process that adapts to varying cognitive and behavioural contexts (*34, 35*). To investigate alterations in hippocampal splitting activity in 5xFAD mice, and its relationship to performance on the alternation task, we first divided the stem arm of the figure-8 maze into 1 cm bins. Place cells with place fields encompassing at least five of these bins on the stem arms were selected. For each of these cells, neural activity rates (standardized amplitude rate) were calculated at each stem bin for every trial. Occupancy tuning curves were constructed for each subsequent correct turn (left and right), and the differences between left and right turn curves were then calculated for each trial. To identify significant splitting activity, we shuffled left-right and right-left trials 1000 times, defining significant splitting as a difference between left and right turn tuning curves exceeding the 95% threshold in the shuffled trials. We observed representative hippocampal CA1 cells showing significant splitting activity for each turn direction in all groups (Fig. 6). To our knowledge, this study presents the first documentation of hippocampal splitter cells in a mouse model of AD during a continuous spatial alternation task.

To further investigate whether 5xFAD mice show impaired splitting activity, we examined four metrics to quantify the quality of splitter cells: 1) Splitting Extent — the proportion of stem bins with significant splitting activity along the stem (*36*). 2) Splitting Discriminability — the magnitude of the disparity between the tuning curves of left and right turns along the entire stem arm (*36*). 3) Splitting Reliability — the trial-to-trial spatial correlations along the stem for trials of the same subsequent turning direction for each neuron along the stem arm. 4) First Splitting Trial — the trial in which a neuron with a stem place field first exhibits significant splitting activity on its preferred turn.

Our results revealed that 5xFAD mice exhibited age-progressive deterioration in all four splitting metrics, indicating impaired splitting activity in the CA1 region. Specifically, 5xFAD mice demonstrated reduced splitting probability, discriminability, and reliability (Figure 7A-C). Moreover, the first occurrence of splitting activity was significantly delayed in 5xFAD mice compared to controls (Figure 7D).

These findings suggest that hippocampal CA1 neurons in 5xFAD mice show degraded splitting activity while performing the alternation task. Additionally, we observed a significant correlation between task performance and the Splitting Extent ($R = 0.57$, $p = 0.001$), Discriminability ($R = 0.60$, $p = 0.0007$), Reliability ($R = 0.45$, $p = 0.013$) and First Splitting Trial occurrence ($R = -0.58$, $p = 0.0009$) (Figure 7E). Taken together, these results

indicate that a specific degradation of hippocampal CA1 splitting activity in 5xFAD mice correlates with deficits in task performance.

Discussion

In our study, we reported a novel head-fixed behavioural paradigm designed for evaluating hippocampal-associated spatial working memory. We used this behavioural paradigm to investigate how Alzheimer's disease related amyloid pathology affects behavioural performance and hippocampal neuronal spatial representations in 5xFAD mice in a continuous spatial alternation task. Previous research has established that the 5xFAD mouse begins to develop amyloid deposits between 2 to 4 months of age, with intraneuronal accumulation of Aβ42 starting as early as 1.5 months (*23*) . This amyloid burden in 5xFAD mice intensifies over their lifespan (*23, 37*). By the time they reach 4 to 6 months of age, these mice exhibit substantial amyloid deposition alongside observed deficits in synaptic transmission, LTP, and sharp wave-ripple events (*22, 23, 38*). While some studies have detected mild impairments in spatial or hippocampus-independent memory as early as 3 to 4 months, more pronounced memory deficits become evident at later stages, beyond 4–6 months of age (*27, 39, 40*). In this study, we did not observe significant deficits in the head-fixed alternation task in 3–4-month-old 5xFAD mice, but old 5xFAD mice (7 to 12 months) displayed significant spatial memory impairments (Fig. 2A).

Behavioural hyperactivity and a disturbance in the relationship between running speed and CA1 neuronal activity are both observed in 5xFAD mice (Supplementary Figures 1,2). Neuronal hyperactivity can lead to behavioural hyperactivity by disrupting neural networks and impairing cognitive functions (*41, 42*), while behavioural hyperactivity can exacerbate neuronal hyperactivity through increased stress and sensory overload. The observation of locomotion linked neuronal activity in our study is crucial, considering that local field potential oscillations in theta and gamma frequencies are closely associated with running speed (*43, 44*). Future investigations could further advance this work by examining the coherence between hippocampal oscillations, calcium activity, running speed, and behavioural trajectories.

Furthermore, our findings align with prior research indicating a decline in hippocampal function in the mouse model of AD (*14-16*). This decline is characterized by reduced spatial information, a lower proportion of place cells, and decreased stability in spatial coding, correlating with the learning and memory deficits observed in 5xFAD mice. Additionally, the stability of place cell activity was found to diminish across trials (Fig. 3), suggesting a weakening in the consistency of spatial memory encoding essential for sequential decision-making tasks. Despite the non-significant deficits observed in young 5xFAD mice, alterations in hippocampal neuronal activity and a marked reduction in spatial representations were observed (Fig. 2E-F). This suggests that significant spatial cognition deficits begin prior to the clear manifestation of cognitive behavioural symptoms in 5xFAD mice.

The stabilisation of place cell coding is believed to be related to the high level of attention required in memory-guided tasks (*45, 46*). While 5xFAD mice are capable of encoding spatial locations, they struggle with reactivating place cells consistently within short intervals between each trial. This old 5xFAD mice may not allocate sufficient attention or integrate sensory, visual, and auditory stimuli into spatial memory coding during the

alternation task. However, although less place cells in 5xFAD maintain consistent significant spatial tuning activity across the learning period, the session-to-session stability in spatial encoding showed that long-term spatial memory might be less affected or subject to a different impairment pattern in 5xFAD mice (Fig. 4).

Crucially, a significant decline in spatially tuned activity near reward locations, indicating a specific vulnerability of reward-related spatial learning in the late stages of AD (Fig. 5). The memory recall of the reward provides the spatial features of the environment, supporting goal directed task performance (*47*). Firstly, rewards provide strong motivation for animals to navigate in space and complete complex cognitive behavioural tasks. The high demands of attention involved in the task could prevent animals from disengaging. Secondly, encoding of the reward location requires sensory and visual stimulus input, which can result in dopaminergic circuit responses. These responses could influence hippocampal cognitive function and synaptic plasticity from the ventral tegmental area (VTA). However, dopaminergic deficits, which we did not investigate in our research, are observed in MCI and AD patients who exhibit neuropsychiatric symptoms (*48, 49*). Consistently, the impairments of spatial encoding of reward position was also prior to behavioural deficits in 5xFAD.

Our study marks the first report of hippocampal splitter cells in a mouse model of AD (Fig. 6) . Splitter cells play an important role in encoding an animal's past experiences and future decisions, integrating within a prefrontal-thalamo hippocampal circuit critical for spatial navigation (*35*). Our findings indicate that hippocampal splitting activity is significantly degraded in 5xFAD mice, a deficit which occurs prior to alternation performance deficits (Figure 7A-D). In addition, degradation of splitting activity was found to correlate with 5xFAD performance deficits (Fig. 7E). Splitter cells, which are integral to task alternation and spatial navigation, likely require recruitment of more complex and more highly integrated neural networks, and possibly greater synaptic plasticity. Our findings give an implication on linking hippocampal splitting activity dysfunction with cognitive impairments in the early stage of AD.

Limitations of the study

This study has several limitations that warrant consideration. First, we did not account for sex differences in our analysis. Human studies indicate that AD prevalence and severity are higher in females, with sex-specific differences observed in amyloid pathology and cognitive decline (*50, 51*). Similar patterns have been reported in the 5xFAD model, with female mice exhibiting greater amyloid deposition and potentially distinct cognitive impairments compared to males (*52-55*). Second, while calcium imaging is a powerful tool for assessing neuronal activity, potential discrepancies in calcium indicator dynamics in AD models must be addressed. Variations in calcium indicator expression, deregulation of calcium signalling, and altered decay kinetics in 5xFAD mice could influence the accuracy of spike inference (*56*).

Materials and Methods

Experimental Animals

5xFAD mice express human APP and PSEN1 transgenes with a total of five AD-linked mutations: the Swedish (K670N/M671L), Florida (I716V), and London (V717I) mutations in APP, and the M146L and L286V mutations in PSEN1. In 5xFAD mice, intraneuronal Aβ was seen in these neurons at 6 weeks and extracellular amyloid plaques were detected in hippocampus at 2 months. Male hemizygous 5xFAD mice (B6SJL-Tg(APPSwFILon, PSEN1∗M146L∗L286V) 6799Vas/Mmjax, JAX stock #034840) were crossed with female homozygous Chat-IRES-Cre(∆neo) mice (JAX stock # 031661) to maintain the 5xFAD+/Chat-IRES-Cre+ and 5xFAD−/Chat-IRESCre+ control groups. Only y118 and y121 were crossed using 5xFAD and wild-type C57BL/6 mice. Colonies under standard animal breeding at Imperial College London. The animal room was kept on a reverse 12:12 lightdark cycle daily.

Ear samples were collected from 5xFAD-Tg and Non-AD transgenic littermates for genotyping identification. Real-time PCR was used for genotyping 5xFAD transgenic with probes APPswTg and huPSEN1Tg, conducted by Transnetyx company. Animals were divided into two age groups: young group aged (young control median age = 3.6 months, N=10; young AD median age = 3.8 months, N=8) and old group aged (old control median age = 8.6 months, N=6, old AD median age = 8.2 months, N=7). Non-AD transgenic littermates were used as controls. Both male and female mice were used for this study. All experimental procedures were carried out under the Animals (Scientific Procedures) Act 1986 and according to Home Office and institutional guidelines, under a Project License to SR Schultz.

Surgeries

Mice were anaesthetised with 1.5-3% isoflurane (Iso-Vet, Chanelle Pharma) and body temperature was maintained at 37 ◦C. Analgesia was administered pre-operatively with Carprofen (5 mg/kg, Rimadyl., Zoetis) and buprenorphine (0.07 mg/kg, Vetergesic., Ceva Animal Health Ltd). Anaesthetic depth was assessed every 10 min for the duration of the experiment by pedal flexion. A small (0.5 mm) craniotomy was made and a cocktail of two Adeno-associated viruses, (pGP-AAV-syn-jGCaMP7s-WPRE, Addgene catalogue 104487-AAV9; pAAV-CAG-tdTomato, Addgene catalogue 59462-AAV9, with the ratio of 3:1) 1 µl was injected into the hippocampus CA1 (at coordinates from bregma, in mm: -1.3 and -1.5 DV, -1.8 ML, -2.0 AP). The first virus delivers a green genetically encoded calcium indicator (jGCaMP7s), and the second an activity-independent red fluorescent protein (tdTomato) which is helpful for tracking cell body movements over time. Ten minutes following viral injection a hippocampal window was implanted as described by Dombeck et al. (*57*). A 3-mm circular craniotomy was made and the cortex (including parietal cortex and parts of visual and hindlimb sensory cortex) above the injection site was aspirated using a 27-gauge needle connected to a water pump until the fibres of the corpus callosum became visible. A stainless steel cannula (diameter: 3 mm, height: 1.5mm) with a glass bottom was pressed down into the tissue and fixed in place using histoacryl glue (B. Braun Surgical). The surrounding skull was roughened using a scalpel blade and a stainless-steel head plate (aperture: 8.5 mm) was glued to the skull, centred on the craniotomy. The exposed skull outside the head plate aperture was covered with dental cement mixed with black powder paint. Mice were given carprofen (5 mg/kg/24 hrs) in oral water for 3 days after surgeries. Mice were allowed 3 weeks to recover before behavioural training began.

Behavioural training in head-fixed mice

Maze apparatus: We used a carbon fibre maze to which were attached visual and tactile cues, and which floated on the Neurotar tracker air table (Mobile HomeCage, Neurotar). This maze features built-in magnets for tracking the animal position within the environments. The maze has a diameter of 32.5 cm. The stem arm (start arm) measures 16 cm in length, while each reward arm and each return arm are 10 cm long. The corridor width of all arms is 5 cm. Visual cues were provided by attached phosphorescent tape, and tactile cues were added using Fiberglass Mesh Tape on the inner wall of the maze. The training cage tape was fully charged with daylight before the commencement of any training sessions.

Handling and habituation: Acclimatization to both the room and maze is crucial for animals to become familiar with the training environment before the commencement of official training sessions. Mice were handled at least two days prior to behavioural training. Animals were required to freely explore in the air-lifted T maze in the training room with red lights on for 10 minutes on the day before training commenced. For the first 5 training days, animals were allowed 5 minutes of free exploration before head fixation.

Water restriction: To motivate mice to navigate and learn the behavioural task, they were subjected to water restriction prior to the first day of training. After 5 days of water restriction, animals' weight stabilized at a little above 85% of initial weight (typically 85 to 90% of baseline body weight) with a daily ration of 40-55 µl/g. During the performance in the training task, if mice did not receive their full ration during the task, supplementary water was provided in their home cage after the second training session finished per day to maintain body weight above 85% of initial weight. Mouse body weight was monitored daily.

Continuous rewarded alternation task: To assess goal directed, hippocampal-dependent spatial memory in the head-fixed mice, we trained them in a continuous rewarded alternation task. Alternations are also referred to as win-shift behaviour. They can reflect the motivation of the mice to explore the environment and location. Animals were trained in the dark during the learning of the alternation task. Infrared (IR) light illuminated the training area, and an IR camera was used to monitor the animals. Animals started running to freely choose one of the reward arms for the first trial. A reward (4 µl) was delivered by a lick spout attached to the head-plate clamp and controlled by a peristaltic pump (Campden Instruments). A reward was accompanied by a beep. In subsequent trials, a reward was given by the spout only when animals entered the goal arm opposite to the arm visited on the previous trial. Mice needed to run forward to complete a trial to get a reward at a fixed reward position. A complete trial was defined by the mouse run-through from the previous trial reward position, return arm, centre arm (stem arm), choice arm, and next reward position sequentially. Head-fixed animals were trained for 45 minutes each session twice a day. Daily training sessions were at least 4 hours apart. The acquisition of our task was defined as 3 consecutive training sessions of performance at or above the criteria of 70% correct. Well performing animals could only be trained for 1 session per day to maintain performance. From the 6th training day, animals received 1% sucrose water as rewards during training and all imaging sessions, but still supplied water for supplementary fluid. The Neurotar Mobile HomeCage tracker (V3.0.0.64) was used for recording mouse positions and behavioural activity data. The figure-8 maze was cleaned with 70% ethanol before each mouse training/imaging recording.

In vivo two-photon Ca^{2+} imaging

Two-photon calcium imaging was performed using a Scientifica resonant scanning microscope with a 16 × Nikon water-immersion objective (LWD 0.8 NA). jGCamp7s and tdTomato fluorophores were excited at 940 nm with a Ti:sapphire laser (Mai Tai HP, Newport). 50% (vol%) ultrasound gel was used as the immersion medium. Images (490 × 490) μm, 512 × 512 pixels field of view) were recorded at 30.9 Hz during imaging sessions using SciScan 1.3 software. Synchronized imaging recording was triggered by a start TTL signal from the behaviour recording software Neurotar. All animals underwent imaging afterwards training days 10th, and some were also imaged on training days 6th and 8th. An imaging session for each mouse did not exceed 2 hours per day. At the start of eah imaging session, mice were head-fixed at the stem arm but restricted by two carbon fibre doors. Once the targeted field of view (FOV) was found (with the same FOV being followed across the training sessions), the two doors were removed, and the mice began began running in the maze, with immediate two-photon imaging recording initiated. We recorded two-photon movies in 4-minute durations for each record file; it typically takes 4-15 files for animals to complete over 80 total trials. To obtain sufficient data for analyzing cellular spatial tuning, the minimum number of total trials stipulated was 80, but usually around 100 trials were obtained.

Behaviour data analysis

Alternation performance： only complete trials (see behaviour training above) were analysed for alternation performance. Although mice would obtain a reward on their first free choice, this initial choice was not included in the count of correct trials. Alternation % was defined as the number of correct trials divided by the total number of trials.

Linearized figure-8 maze trajectory

To obtain linearized moving trajectories, we first segmented the figure-8 maze into four functional sections. The trajectory was parsed into different sections, starting at the return arm, then moving up the stem arm into the choice arm, and finally entering the reward arm. The rewarded spout location was the boundary between the choice and reward arms. Next, we divided the overall trajectories into LR, RL, LL, and RR trials with maze segmentation. Ultimately, the trajectory was linearized by trial types into a 49.5 cm length track, the estimated length of a complete trial. Trials were sorted by the order of completed trials when the mouse moved in the maze.

Imaging data processing

To extract individual neurons' calcium activity, we employed a customised image processing pipeline using a MATLAB implementation of the CaImAn package (*58*), following the protocol outlined in Go et al. (*59*). Initially, we performed rigid image registration followed by non-rigid image registration to correct for motion artifacts in the imaging videos. Once the images were registered to a template from the same session, regions of interest (ROIs) were identified, excluding any overlapping ROIs. To track ROIs across multiple sessions, we registered images from different sessions to a template from one session, identifying ROIs on the temporally concatenated video. For measuring single-neuron calcium amplitude trains, we performed neural activity deconvolution using sparse non-negative deconvolution. This was implemented with an exponential kernel of decay timescale appropriate to the sensor used, utilizing the OASIS (Online Active Set method to Infer Spikes) algorithm to convert calcium activity into trains with both onset times and amplitudes.

Amplitude standardisation

To eliminate out any discrepancies in OASIS event amplitude between different mice and FOVs, we fitted the distribution of event amplitudes for each FOV in each mouse to a lognormal distribution and standardised the distribution for each FOV to unit mean. This eliminates variability in event amplitude due to differences in signal to noise ratio (for instance due to imaging depth, viral expression, or tissue age), and makes it possible to compare calcium activity rates objectively across FOVs and animals. The units of the resulting deconvolved calcium event amplitudes are arbitrary, however they are identical arbitrary units across the entire dataset.

Place cell identification

The Figure-8 maze was discretized into 1 cm-wide bins, forming a 32 x 32 grid, to construct spatial rate maps. For each bin, we calculated the spatial activity rate by dividing the sum of the standardised deconvolved calcium amplitudes collected from that bin by the total time the mouse spent in that bin, only including running speeds larger than 8 mm/s. We employed a Gaussian kernel with a sigma value of [3,3] to smooth the spatial rate maps. The spatial information content of each neuron was calculated using Skaggs's spatial information method [36] (bits per arb, standardised amplitude rate), is calculated using the following formula:

$$\mathrm{SI} = \sum_{i=1}^{N} P_i \frac{\lambda_i}{\lambda} log_2 \left(\frac{\lambda_i}{\lambda}\right)$$

where SI is the spatial information in bits/arb. P_i is the probability of the mouse being in the i-th bin. λ_i is the mean standardised amplitude rate of the cell when the mouse in the *i*-th bin. λ is the overall mean standardised amplitude rate of the cell across the entire environment. N is the total number of spatial bins. 2D place cells within the Figure-8 maze were identified based on the following criteria: 1) A neuron's SI must exceed the 95th percentile of the shuffled SI values, 2) the neuron should be active within the place field for more than 2% of the time the mouse spends in that field, and 3) the size of the place field must exceed 5 cm^2. The boundary of a place field was determined by encompassing all connected occupancy bins where the smoothed rate amplitude was at least 50% of the peak rate in the occupancy bin. For 1D place cells selection, we calculated for total, rl, lr, ll and rr trials respectively. The criterions for 1D place cells: 1) spatial information need to in the top of 5 % shuffled spatial information. 2) cells active time percent of time spent in place field should be at least 1 %. 3) cells active more than 30% of total number of trials.

Splitter cell identification

The identification of splitter cells involved segmenting figure-8 trajectories into return, stem, choice, and reward sections. The stem arm was further divided into 1 cm bins. Place cells spanning at least five bins on the stem arms were selected. For each cell, the neural activity rate was calculated at each stem bin for every trial. Occupancy tuning curves were constructed for each correct turn (left and right), and the differences between left and right turn curves for each trial were calculated. Significant splitter cells were identified through a shuffling process of left-right and right-left trials 1000 times. A significant splitter cell was defined as a neuron with place fields in at least five stem arm bins, one of bins whose tuning curve difference exceeded the 95% threshold in the shuffled trial results.

Trajectory-dependent activity quality

The quality of trajectory-dependent neuronal activity was described by three metrics applied to analyze the activity of cells located along the stem arms with place fields on the stem arm (*36*). Discriminability: It involves summing the absolute values of the differences between these tuning curves across all stem bins, normalized by dividing by the aggregate sum of the tuning curves across all stem bins. Reliability: Assessed using a shuffling permutation

test, where trial identities were shuffled 1,000 times. Reliability is a metric that quantifies the consistency of spatial correlations in preferred turning direction across trials for each neuron along the entire stem arm. The trial-to-trial correlations for splitting activity were calculated based on the encoded trajectory activity of the neurons. Specifically, we computed the Spearman correlation coefficients between the spatial activity bins of adjacent trajectory trials within the same imaging session. For example, if a neuron exhibited splitting activity along the stem arm bins and showed a preferred firing direction during left-right (L-R) trials, we then calculated the trial-to-trial correlation between the spatial activity of adjacent L-R trials. Splitting Extent: Defined as the proportion of stem bins that demonstrated a statistically significant disparity between the left and right tuning curves, where 'significant difference' implies the actual difference in a given bin exceeded the difference in 95% of the corresponding shuffled bins.

Statistical tests

Mouse behaviour data and pathology were presented as mean ± SEM unless otherwise specified. Appropriate statistical analyses were applied based on the experimental design. These included Analysis of Variance (ANOVA), Kruskal-Wallis (K-W), and Mann-Whitney U (MWU) tests. All statistical analyses were conducted in MATLAB, with significance levels set at $p \leq 0.05$.

Acknowledgments

We thank Yu Liu and Nawal Zabouri for their help with animal genotyping and daily support, Jina Song for assisting with the behavioral training protocol, and Seigfred Prado for his help with image processing using high-performance computing.

Funding:

Mrs Anne Uren and the Michael Uren Foundation to SRS
EPSRC EP/W024020/1 and EP/W035057/1 to SRS
BBSRC BB/Y514202/1 to SRS
CZI CP-2-1-Schultz to SRS
China Scholarship Council CSC scholarship to YL

Author contributions:

Y.L. conceived the study and mainly conducted experiments and collected data under guidance and supervision of S.R.S. and M.A.G., Y.L. and H.Z. analyzed data. M.A.G. and H.Z. contributed to imaging data processing. Y.L. and S.R.S. wrote the paper. All authors discussed and commented on the manuscript.

Competing interests: Authors declare that they have no competing interest.

Data and materials availability: Code and data used to generate the figures described in this paper will be made available via DataDryad at the time of publication, with a DOI to be included here.

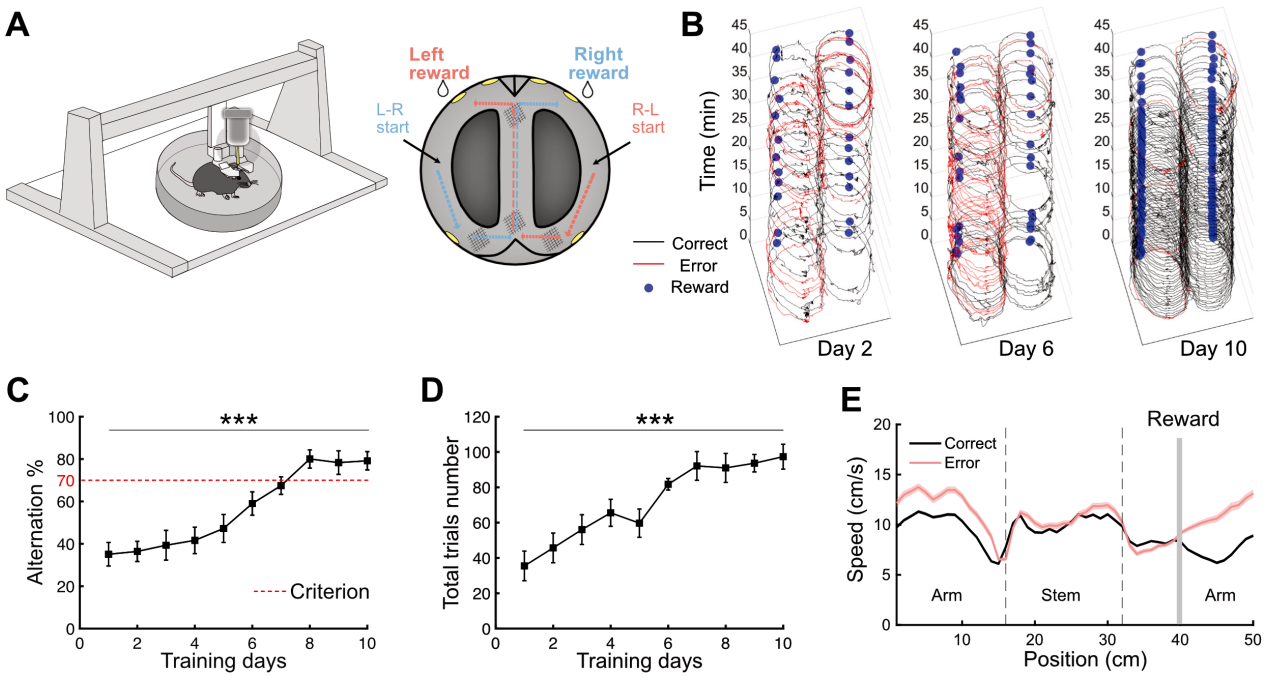

Figure 1. Head-fixed mice learn in a continuous spatial alternation task

A. Left: Schematic showing a head-fixed mouse in the behavioural apparatus. Right: The bird's eye view schematic of the air-lifted figure-8 maze. Correct trials: from left to right arm (blue), from right to left arm (red).

B. Temporal tracking of mouse position, differentiating between correct trials (black lines) and error trials (red lines) on the 2nd, 6th and 10th days of training, with reward locations demoted by blue dots.

C. The number of total trials across the training in head-fixed mice (N=10) enhanced significantly ($F_{(9, 99)} = 8.93$, $P = 1.7 \times 10^{-9}$, One-Way ANOVA test).

D. Alternation percentage across the training improved in head-fixed mice (N=10, $F_{(9, 99)} = 11.58$, $P = 7.0 \times 10^{-12}$, One-Way ANOVA test). Horizon dots line represents the criterion score (70%) for acquisition of the task.

E. Animal speed during correct (black) and error (red) trials in the linearized trajectories calculated in 1 cm spatial bins. The vertical line marks the start and end of the central arm. Reward spout position is indicated in grey shadow. Linearized position (0 cm) starts are shown on the right of (A). $***$ indicate the significance levels with p values < 0.0001.

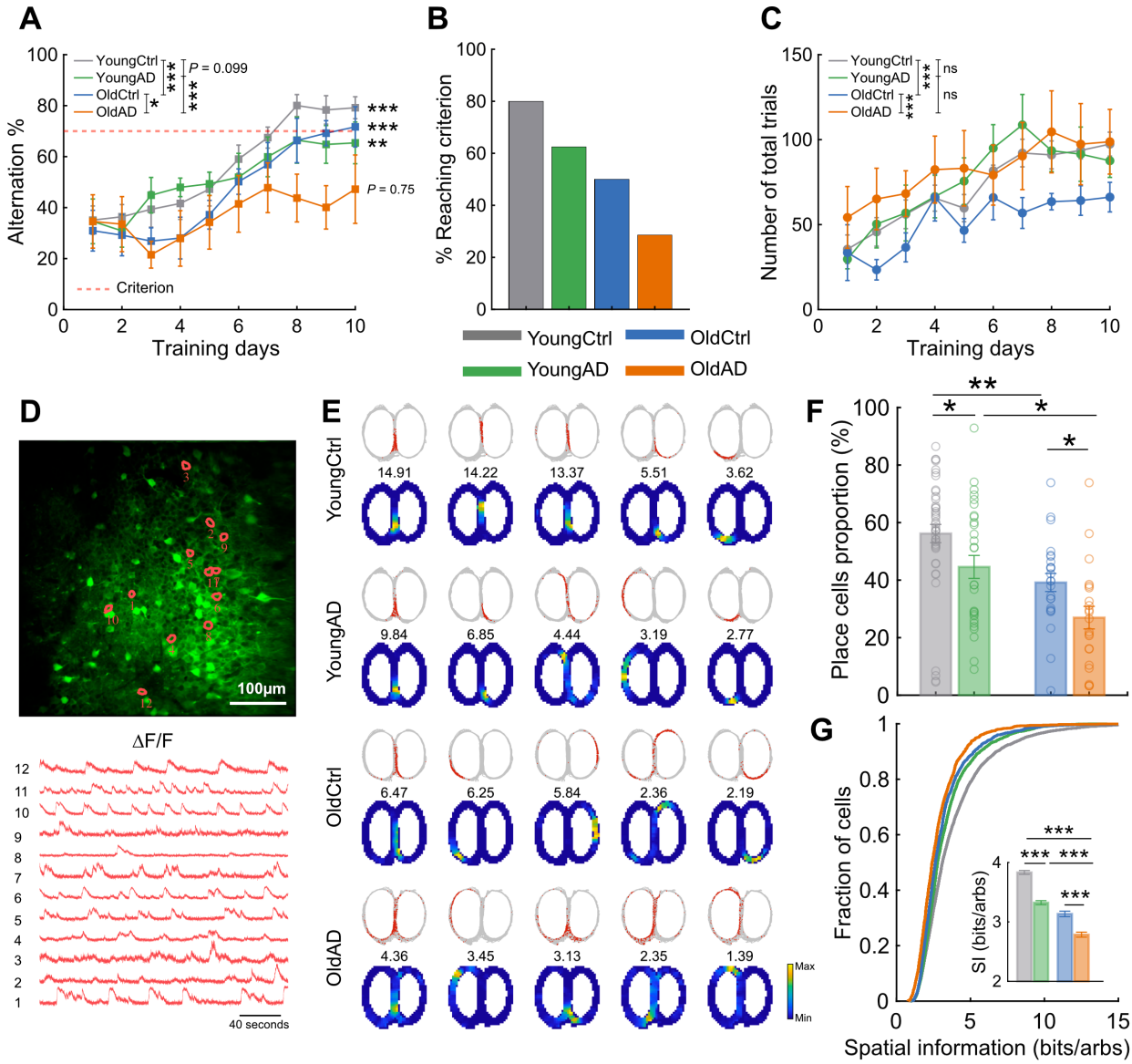

Figure 2: 5xFAD mice showed age-progressive deficits in behavioural performance and spatial representations

A. Percentage of correct alternations on each training day for all experimental groups. Young control (grey), Young 5XFAD (green), Old control (blue), Old 5xFAD (orange). Horizontal red dotted line indicates criterion (70%) for task acquisition. One-way ANOVA test for each animal group across days. Two-way ANOVA test for group comparison.

B. Percentage of mice successfully acquiring the alternation task within 10 days for all groups.

C. Total number of trials achieved per day for animals from all experimental groups. Age-dependent increase in the number of trials completed by 5xFAD mice throughout training days, indicating significant AD effect ($F_{(1,330)} = 10.9$, $P = 0.001$) and AD × Age effect ($F_{(1,330)} = 7.3$, $P = 0.007$). Two-way ANOVA test.

D. Top: representative FOV (490 × 490 µm) of hippocampal CA1 region expressing jGCaMP7s. 12 randomly selected ROIs overlaid on the image in red. Bottom: Raw ΔF/F temporal traces from corresponding neurons in top.

E. Five representative CA1 place cells in young control, young 5xFAD, old control and old 5xFAD, respectively. Raster plots (upper panels) and normalized neural activity rate map (lower panels); Skagg's spatial information (bits/arb) is indicated for each representative place cell.

F. The percentage of neurons meeting "place cell" criteria was reduced in 5xFAD mice. Scheirer-Ray-Hare test with post-hoc test with Bonferroni correction.

G. Spatial information (Skaggs measure, bits/arb) showed progressive decrease with age in 5xFAD mice. Scheirer-Ray-Hare test with post-hoc test with Bonferroni correction. $*$, $**$ and $***$ indicate significance levels with the respective p values of < 0.05, < 0.005 and < 0.0001.

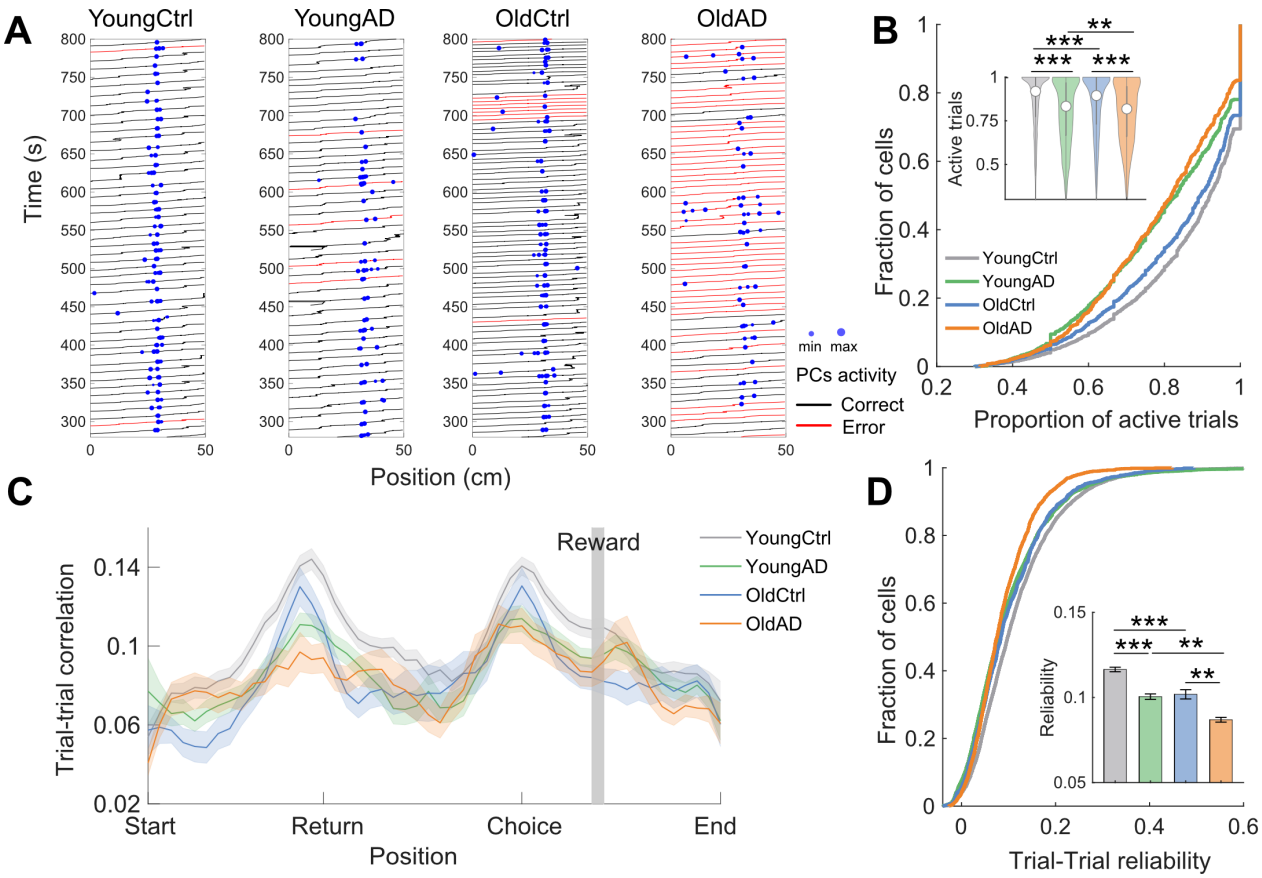

Figure 3: Impaired trial-to-trial reliability of spatial tuning activity in 5xFAD mice

A. Temporal tracking of mouse linearized position, showing typical examples of place cell activity throughout trajectories during each trial. Black line: position on correct trials, Red line: position on error trials, Blue dots: Place cell activity.

B. Proportion of trials in which place cells were active diminished in 5xFAD mice. Cumulative plots with inset violin plots illustrate the proportion of trials in which place cells were active across all imaging sessions. Violin plots show median, minimum and maximum values. Scheirer-Ray-Hare test with Bonferroni post hoc test.

C. Trial-to-trial correlation (mean adjacent trial-to-trial Spearman correlation of spatially binned activity) of CA1 spatial tuning across position, for each mouse group. Shading represents mean ± s.e.m. across cells.

D. Mean Trial-to-trial correlation of place cells (average of trial-trial correlation across all spatial bins in each cells) age-dependently decreased in 5xFAD mice. Scheirer-Ray-Hare test with Bonferroni post hoc test, mean ± s.e.m.., ∗, ∗∗ and ∗ ∗ ∗ indicate the significance levels with the respective p values of < 0.05, < 0.005 and < 0.0001. See also Table S1.

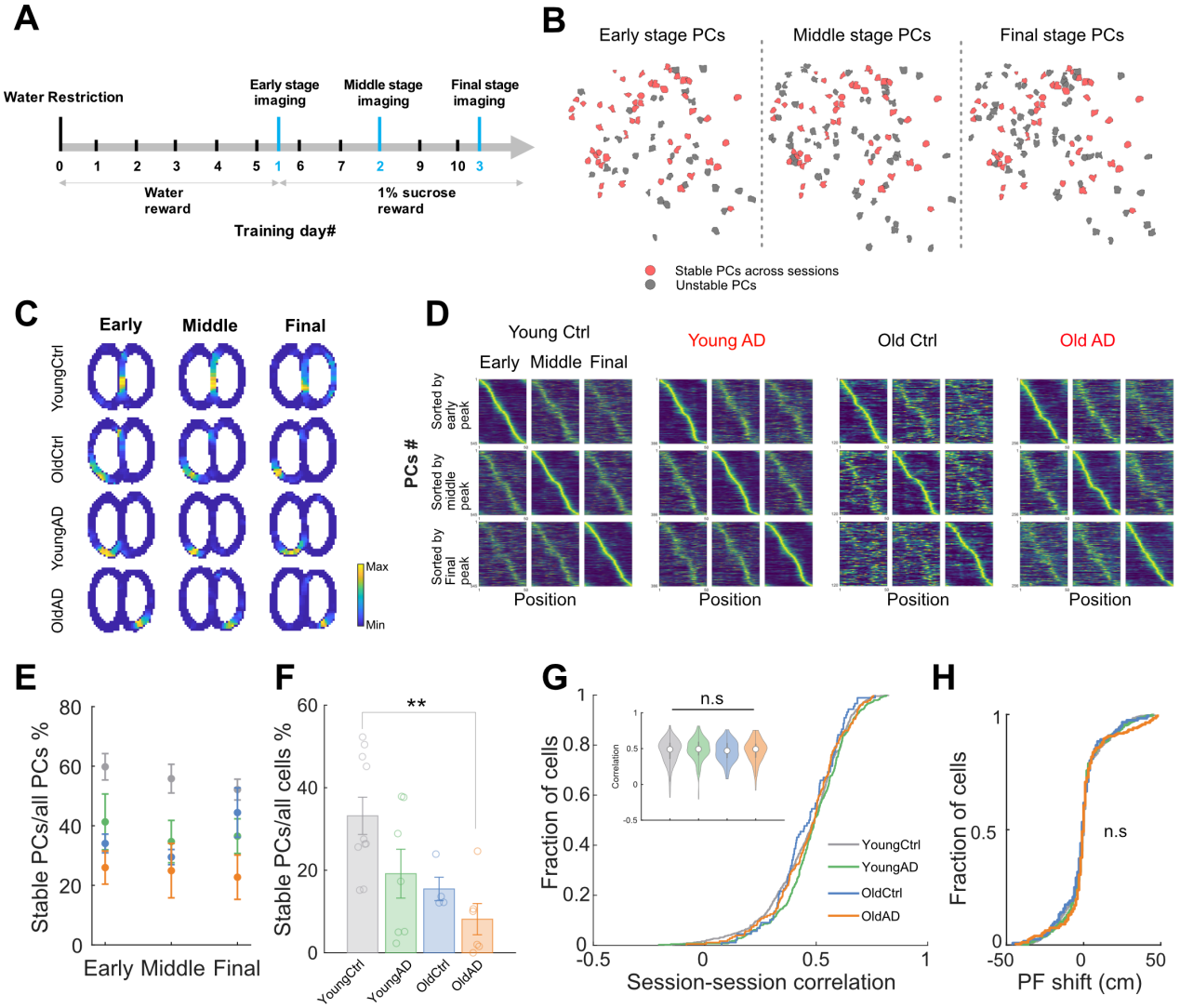

Figure 4. Number of place cells in 5xFAD mice reduced across sessions but stable place fields maintained.

A. The timeline of the imaging sessions across the training task, including early-stage imaging (around the 6th training day), middle stage imaging (around the 8th training day), and final stage imaging (after the 10th training day).

B. Place cells from an example FOV during the early, middle and final stage, with red contours indicating place cells in this session and red contours highlighting place cells that maintained spatial tuning activity across early, middle, and final stages (Stable place cells).

C. Representative spatial maps for stable place cells throughout the training phase in both control and 5xFAD mice.

D. Distribution of place fields along a linear trajectory, sorted by place cells at each experimental stage.

E. The proportion of place cells that persisted across all stages (stable place cells) to the number of all place cells (PCs) identified at each individual stage. The stable PC proportion was reduced in old 5xFAD mice compared to young Ctrl mice. See detailed statistical results in Table S1.

F. Proportion of stable place cells to the number of all tracked cells across sessions.

G. Session-to-session spatial correlation coefficients of stable place cells in all mouse groups. 5xFAD mice did not show reduced spatial correlations. Scheirer-Ray-Hare test, AD effect: $p = 0.34$, Age effect: $p = 0.10$. n.s, not significant.

H. Place field shift of stable place cells from early stage to final stage in control and 5xFAD mice, Scheirer-Ray-Hare test, Age effect: $p=0.15$, AD effect: $p=0.89$. n.s, not significant. $**$ indicate the significance levels with the p values of < 0.005. See also Table S1.

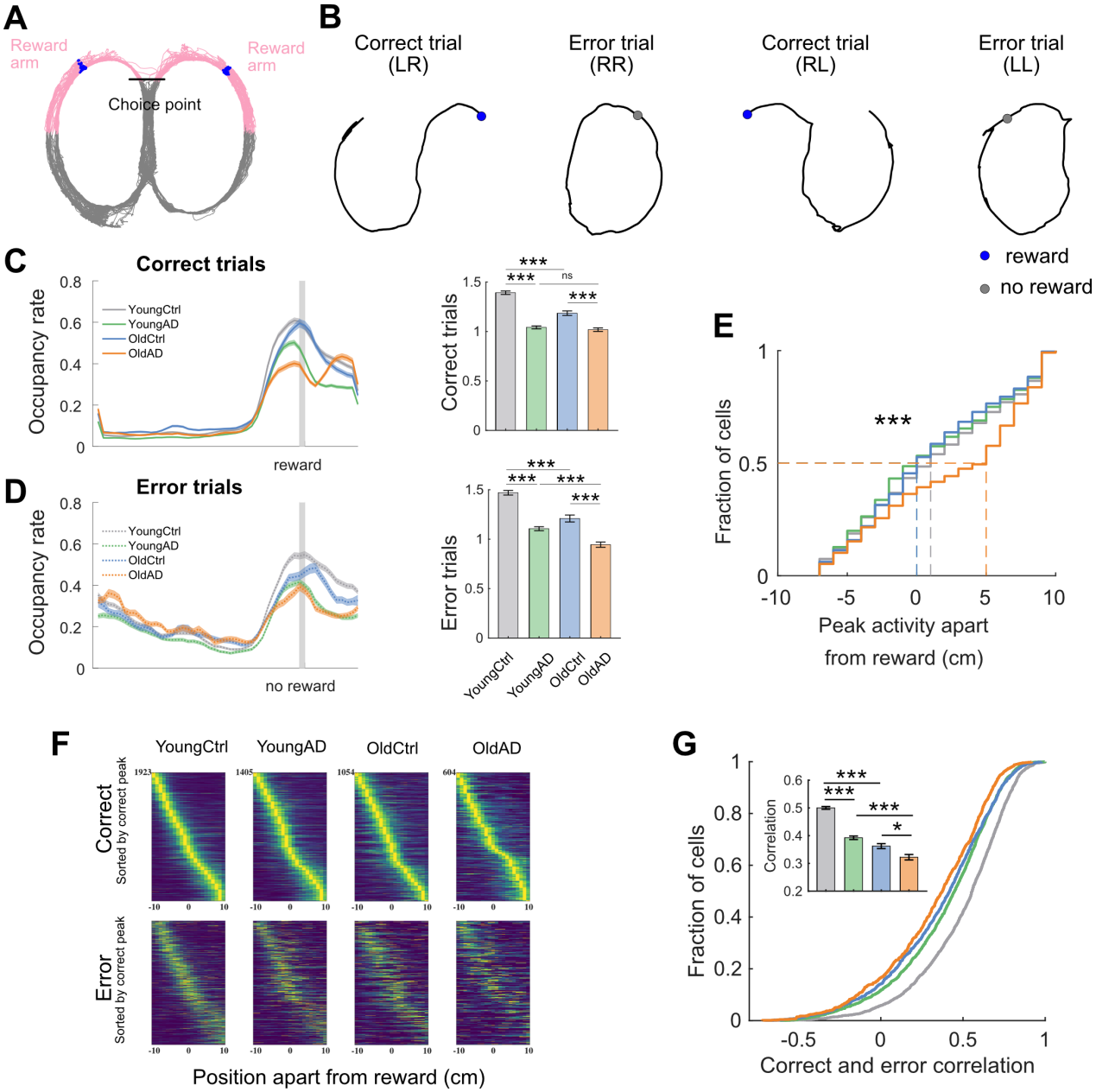

Figure 5: 5xFAD place cells show reduced activity in the reward arm

A. Typical mouse trajectory in a continuous alternation task session. Choice-reward arm (pink), reward location (blue), and other arms (grey) are indicated.
B. Example of mouse trajectory on correct trials and error trials from previous reward location to next one. Rewarded location is marked by blue dots, no reward location is marked by grey dots.
C. Occupancy rates of reward-arm place cells during correct trials. Shading represents mean ± s.e.m. across cells. Two-way ANOVA test with Tukey post hoc test.
D. Same as **C.** but for error trials.
E. Deviation in peak activity location from the reward spout position in reward cells. Kruskal-Wallis test with Bonferroni post hoc test.
F. Normalized peak place cell activity along reward arm position. Top: correct trials, Bottom: error trials. Sorted by peak activity during correct trials.

G. Cumulative plots with inset bar plots illustrate the spatial correlation of reward-arm place cell activity between correct and error trials was reduced in 5xFAD mice. Bar plots show data as mean ± s.e.m.. Two-way ANOVA test with Tukey post hoc test. $*$, $**$ and $***$ indicate significance levels with respective p values of < 0.05, < 0.005 and < 0.0001. See also Table S1.

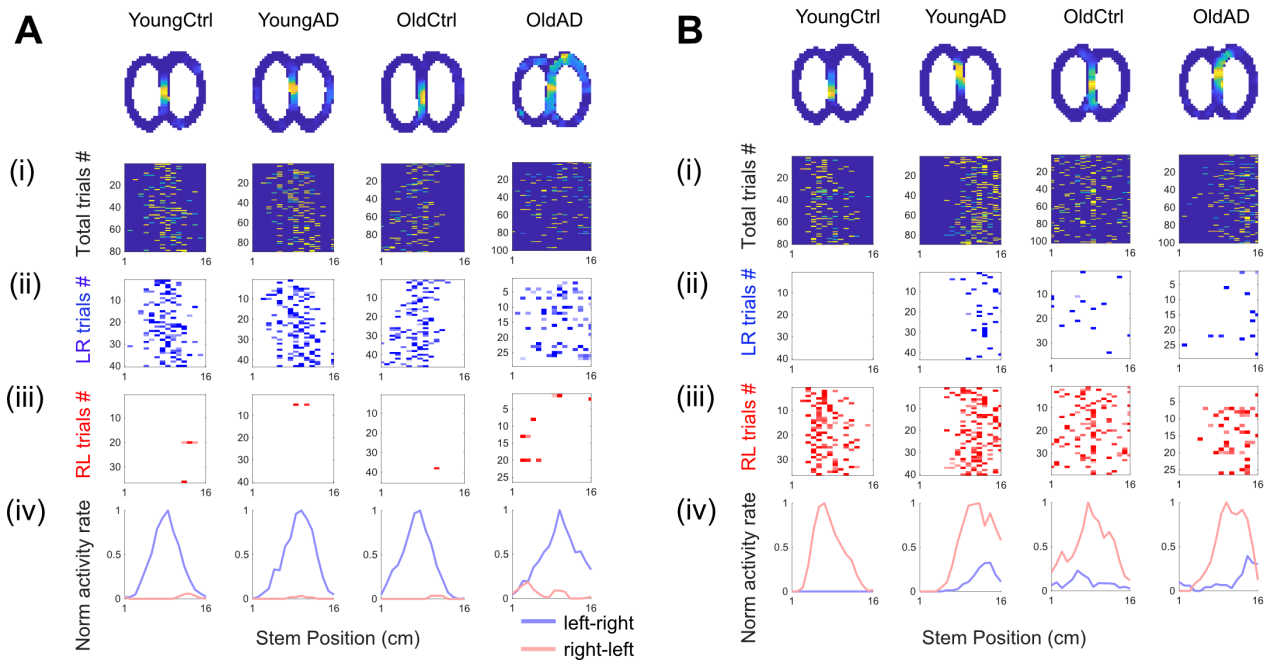

Figure 6. Representative CA1 cells with splitting activity.

A. Four representative stem place cells, one for each group. Each column, top to bottom: (i) Normalized calcium activity occupancy 2D map for the figure-8 maze for one imaging session; (ii) Neuronal calcium activity raster along the stem for all trials at linear figure-8 maze from same imaging session; (iii) Neuronal calcium activity raster along the stem for all left-right trials (blue) from same imaging session; (iv) Neuronal calcium activity raster along the stem for all left-right trials (red) from same imaging session; (iv) Normalised calcium tuning curves for each turn direction. blue: left-right turn, red: right-left turn.

B. As for **A** but for representative splitter cells dependent on right-left turns.

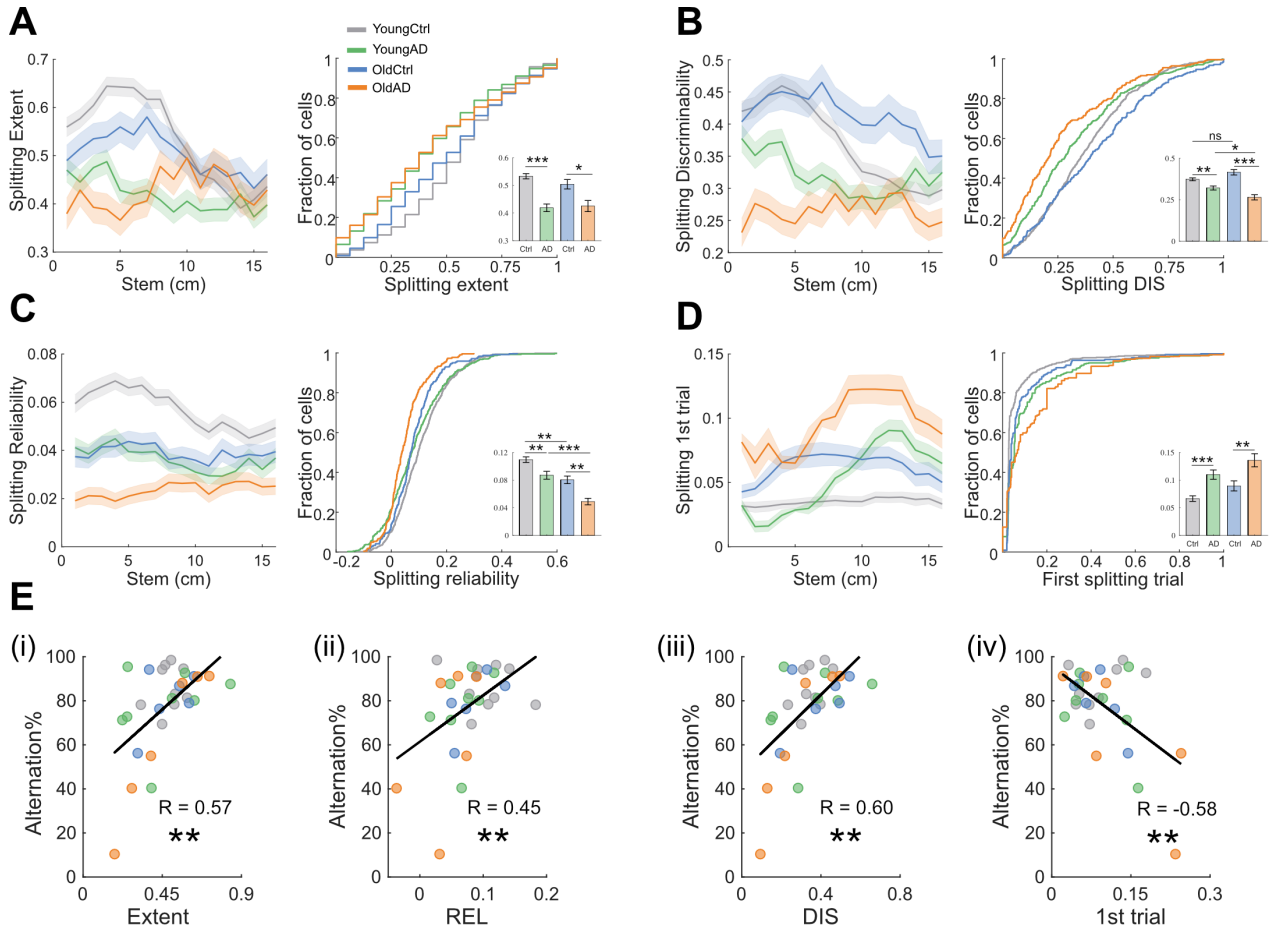

Figure 7: Splitting activity degraded in 5xFAD mice.

A. Splitting Extent was reduced in 5xFAD mice. Left panel: splitting extent pooled across all neurons in each group for each stem spatial bin. Right panel: cumulative histogram with inset bar plots (mean ± s.e.m.) illustrate the mean splitting extent across all stem bins for each neuron from the four mouse groups.

B. Splitting Discriminability was impaired in 5xFAD mice. Left: Splitting Discriminability pooled from all neurons in each group for each stem spatial bin. Right: The cumulative distribution with inset bar plots (mean ± s.e.m.) illustrate the mean Splitting Discriminability across all stem bins for each neuron from the four mouse groups.

C. Splitting reliability was degraded in 5xFAD mice. Left: Splitting Reliabiilty pooled from all neurons in each group for each stem spatial bin. Right: Cumulative distribution with inset bar plots (mean ± s.e.m.) illustrate the mean Splitting Reliability across all stem bins for each neuron from the four mouse groups.

D. The first splitting trial occurrence tended to occur significantly later in 5xFAD mice. Left panel: normalised incidence of first splitting trial, pooled across neurons in each group for each stem spatial bin. Right: Cumulative distribution with inset bar plots (mean ± s.e.m.) illustrate the mean normalised incidence of first splitting trial across all stem bins for each neuron from the four mouse groups.

E. Splitting quality metrics correlate with animal behaviour. (i) Splitting Extent correlates with alternation performance. R = 0.57, p = 0.001. (ii) Splitting discriminability. R = 0.60, p = 5.6×10^{-4}. (iii) Splitting Reliability (mice in which stem place cells were not detected were excluded). R = 0.45, p = 0.013. (iv) Normalized incidence of first splitting trial negatively correlates with alternation performance. R = −0.58, p = 9.2×10^{-4}.

Pearson correlation. $*$, $**$ and $***$ indicate the significance levels with the respective p values of < 0.05, < 0.005 and < 0.0001. See also Table S1.

References

1. A. A. Tahami Monfared, M. J. Byrnes, L. A. White, Q. Zhang, Alzheimer's Disease: Epidemiology and Clinical Progression. *Neurol Ther* **11**, 553-569 (2022).
2. M. A. Busche, B. T. Hyman, Synergy between amyloid-β and tau in Alzheimer's disease. *Nature Neuroscience* **23**, 1183-1193 (2020).
3. H. Xiong *et al.*, Cholesterol retention in Alzheimer's brain is responsible for high β-and γ-secretase activities and Aβ production. *Neurobiology of disease* **29**, 422-437 (2008).
4. C. Condello, P. Yuan, A. Schain, J. Grutzendler, Microglia constitute a barrier that prevents neurotoxic protofibrillar Aβ42 hotspots around plaques. *Nat. Commun.* **6**, 6176 (2015).
5. B. Bellaver *et al.*, Astrocyte reactivity influences amyloid-β effects on tau pathology in preclinical Alzheimer's disease. *Nature medicine* **29**, 1775-1781 (2023).
6. S. Frere, I. Slutsky, Alzheimer's Disease: From Firing Instability to Homeostasis Network Collapse. *Neuron* **97**, 32-58 (2018).
7. W. W. Yau *et al.*, Longitudinal assessment of neuroimaging and clinical markers in autosomal dominant Alzheimer's disease: a prospective cohort study. *Lancet Neurol* **14**, 804-813 (2015).
8. K. B. Rajan, R. S. Wilson, J. Weuve, L. L. Barnes, D. A. Evans, Cognitive impairment 18 years before clinical diagnosis of Alzheimer disease dementia. *Neurology* **85**, 898-904 (2015).
9. J. Hort *et al.*, Spatial navigation deficit in amnestic mild cognitive impairment. *Proceedings of the National Academy of Sciences* **104**, 4042-4047 (2007).
10. T. Hope *et al.*, The structure of wandering in dementia. *International Journal of Geriatric Psychiatry* **9**, 149-155 (1994).
11. Y. Vyas, J. M. Montgomery, J. E. Cheyne, Hippocampal deficits in amyloid-β-related rodent models of Alzheimer's disease. *Frontiers in neuroscience* **14**, 266 (2020).
12. M. J. West, P. D. Coleman, D. G. Flood, J. C. Troncoso, Differences in the pattern of hippocampal neuronal loss in normal ageing and Alzheimer's disease. *The lancet* **344**, 769-772 (1994).
13. E. J. Mufson *et al.*, Hippocampal plasticity during the progression of Alzheimer's disease. *Neuroscience* **309**, 51-67 (2015).
14. F. Cacucci, M. Yi, T. J. Wills, P. Chapman, J. O'Keefe, Place cell firing correlates with memory deficits and amyloid plaque burden in Tg2576 Alzheimer mouse model. *Proceedings of the National Academy of Sciences* **105**, 7863-7868 (2008).
15. R. Zhao, S. W. Fowler, A. C. Chiang, D. Ji, J. L. Jankowsky, Impairments in experience-dependent scaling and stability of hippocampal place fields limit spatial learning in a mouse model of Alzheimer's disease. *Hippocampus* **24**, 963-978 (2014).
16. A. J. Mably, B. J. Gereke, D. T. Jones, L. L. Colgin, Impairments in spatial representations and rhythmic coordination of place cells in the 3xTg mouse model of Alzheimer's disease. *Hippocampus* **27**, 378-392 (2017).
17. X. Lin *et al.*, Spatial coding defects of hippocampal neural ensemble calcium activities in the triple-transgenic Alzheimer's disease mouse model. *Neurobiology of disease* **162**, 105562 (2022).
18. S. M. Prince *et al.*, Alzheimer's pathology causes impaired inhibitory connections and reactivation of spatial codes during spatial navigation. *Cell reports* **35**, (2021).
19. H. Jun *et al.*, Disrupted place cell remapping and impaired grid cells in a knockin model of Alzheimer's disease. *Neuron* **107**, 1095-1112. e1096 (2020).

20. E. R. Wood, P. A. Dudchenko, R. J. Robitsek, H. Eichenbaum, Hippocampal neurons encode information about different types of memory episodes occurring in the same location. *Neuron* **27**, 623-633 (2000).
21. L. M. Frank, E. N. Brown, M. Wilson, Trajectory encoding in the hippocampus and entorhinal cortex. *Neuron* **27**, 169-178 (2000).
22. R. Kimura, M. Ohno, Impairments in remote memory stabilization precede hippocampal synaptic and cognitive failures in 5XFAD Alzheimer mouse model. *Neurobiology of disease* **33**, 229-235 (2009).
23. H. Oakley *et al.*, Intraneuronal β-amyloid aggregates, neurodegeneration, and neuron loss in transgenic mice with five familial Alzheimer's disease mutations: potential factors in amyloid plaque formation. *Journal of Neuroscience* **26**, 10129-10140 (2006).
24. L. Devi, M. Ohno, Cognitive benefits of memantine in Alzheimer's 5XFAD model mice decline during advanced disease stages. *Pharmacol Biochem Behav* **144**, 60-66 (2016).
25. D. S. Roy *et al.*, Memory retrieval by activating engram cells in mouse models of early Alzheimer's disease. *Nature* **531**, 508-512 (2016).
26. M. S. Pádua, J. L. Guil-Guerrero, P. A. Lopes, Behaviour Hallmarks in Alzheimer's Disease 5xFAD Mouse Model. *International Journal of Molecular Sciences* **25**, 6766 (2024).
27. S. D. Girard *et al.*, Onset of hippocampus-dependent memory impairments in 5XFAD transgenic mouse model of Alzheimer's disease. *Hippocampus* **24**, 762-772 (2014).
28. S. M. Kim, L. M. Frank, Hippocampal lesions impair rapid learning of a continuous spatial alternation task. *PLoS One* **4**, e5494 (2009).
29. R. Gerlai, A new continuous alternation task in T-maze detects hippocampal dysfunction in mice. A strain comparison and lesion study. *Behav Brain Res* **95**, 91-101 (1998).
30. T. Wang *et al.*, Locomotor hyperactivity in the early-stage Alzheimer's disease-like pathology of APP/PS1 mice: associated with impaired polarization of astrocyte aquaporin 4. *Aging and Disease* **13**, 1504 (2022).
31. B. Kim, G. O. Noh, K. Kim, Behavioural and psychological symptoms of dementia in patients with Alzheimer's disease and family caregiver burden: a path analysis. *BMC geriatrics* **21**, 1-12 (2021).
32. C. Lever, T. Wills, F. Cacucci, N. Burgess, J. O'Keefe, Long-term plasticity in hippocampal place-cell representation of environmental geometry. *Nature* **416**, 90-94 (2002).
33. Y. Ziv *et al.*, Long-term dynamics of CA1 hippocampal place codes. *Nat Neurosci* **16**, 264-266 (2013).
34. J. A. Ainge, M. A. van der Meer, R. F. Langston, E. R. Wood, Exploring the role of context-dependent hippocampal activity in spatial alternation behavior. *Hippocampus* **17**, 988-1002 (2007).
35. H. T. Ito, S. J. Zhang, M. P. Witter, E. I. Moser, M. B. Moser, A prefrontal-thalamo-hippocampal circuit for goal-directed spatial navigation. *Nature* **522**, 50-55 (2015).
36. N. R. Kinsky *et al.*, Trajectory-modulated hippocampal neurons persist throughout memory-guided navigation. *Nat Commun* **11**, 2443 (2020).
37. K. L. Youmans *et al.*, Intraneuronal Aβ detection in 5xFAD mice by a new Aβ-specific antibody. *Molecular neurodegeneration* **7**, 1-14 (2012).
38. N. Crouzin *et al.*, Area-specific alterations of synaptic plasticity in the 5XFAD mouse model of Alzheimer's disease: dissociation between somatosensory cortex and hippocampus. *PloS one* **8**, e74667 (2013).
39. A. J. Martorell *et al.*, Multi-sensory gamma stimulation ameliorates Alzheimer's-associated pathology and improves cognition. *Cell* **177**, 256-271. e222 (2019).

40. H. Zhang *et al.*, Degenerate mapping of environmental location presages deficits in object-location encoding and memory in the 5xFAD mouse model for Alzheimer's disease. *Neurobiology of disease* **176**, 105939 (2023).
41. A. M. Miranda *et al.*, Excess synaptojanin 1 contributes to place cell dysfunction and memory deficits in the aging hippocampus in three types of Alzheimer's disease. *Cell reports* **23**, 2967-2975 (2018).
42. M. A. Busche *et al.*, Critical role of soluble amyloid-beta for early hippocampal hyperactivity in a mouse model of Alzheimer's disease. *Proc Natl Acad Sci U S A* **109**, 8740-8745 (2012).
43. L. L. Colgin, Rhythms of the hippocampal network. *Nature Reviews Neuroscience* **17**, 239-249 (2016).
44. T. Ridler, J. Witton, K. G. Phillips, A. D. Randall, J. T. Brown, Impaired speed encoding and grid cell periodicity in a mouse model of tauopathy. *Elife* **9**, e59045 (2020).
45. R. Zemla, J. J. Moore, M. D. Hopkins, J. Basu, Task-selective place cells show behaviorally driven dynamics during learning and stability during memory recall. *Cell reports* **41**, (2022).
46. C. G. Kentros, N. T. Agnihotri, S. Streater, R. D. Hawkins, E. R. Kandel, Increased attention to spatial context increases both place field stability and spatial memory. *Neuron* **42**, 283-295 (2004).
47. M. Sosa, L. M. Giocomo, Navigating for reward. *Nat Rev Neurosci* **22**, 472-487 (2021).
48. X. Pan *et al.*, Dopamine and dopamine receptors in Alzheimer's disease: a systematic review and network meta-analysis. *Frontiers in aging neuroscience* **11**, 175 (2019).
49. P. Krashia, E. Spoleti, M. D'Amelio, The VTA dopaminergic system as diagnostic and therapeutical target for Alzheimer's disease. *Frontiers in Psychiatry* **13**, 1039725 (2022).
50. M. Arnold *et al.*, Sex and APOE ε4 genotype modify the Alzheimer's disease serum metabolome. *Nat. Commun.* **11**, 1148 (2020).
51. D. Sohn *et al.*, Sex differences in cognitive decline in subjects with high likelihood of mild cognitive impairment due to Alzheimer's disease. *Scientific reports* **8**, 7490 (2018).
52. C. H. Poon *et al.*, Sex differences between neuronal loss and the early onset of amyloid deposits and behavioral consequences in 5xFAD transgenic mouse as a model for Alzheimer's disease. *Cells* **12**, 780 (2023).
53. K. R. Sadleir, W. A. Eimer, S. L. Cole, R. Vassar, Aβ reduction in BACE1 heterozygous null 5XFAD mice is associated with transgenic APP level. *Molecular neurodegeneration* **10**, 1-16 (2015).
54. T. P. O'Leary, R. E. Brown, Visuo-spatial learning and memory impairments in the 5xFAD mouse model of Alzheimer's disease: Effects of age, sex, albinism, and motor impairments. *Genes, Brain and Behavior* **21**, e12794 (2022).
55. A. L. Oblak *et al.*, Comprehensive evaluation of the 5XFAD mouse model for preclinical testing applications: a MODEL-AD study. *Frontiers in aging neuroscience* **13**, 713726 (2021).
56. E. Popugaeva, E. Pchitskaya, I. Bezprozvanny, Dysregulation of intracellular calcium signaling in Alzheimer's disease. *Antioxidants & redox signaling* **29**, 1176-1188 (2018).
57. D. A. Dombeck, C. D. Harvey, L. Tian, L. L. Looger, D. W. Tank, Functional imaging of hippocampal place cells at cellular resolution during virtual navigation. *Nat Neurosci* **13**, 1433-1440 (2010).
58. A. Giovannucci *et al.*, CaImAn an open source tool for scalable calcium imaging data analysis. *Elife* **8**, e38173 (2019).
59. M. A. Go *et al.*, Place cells in head-fixed mice navigating a floating real-world environment. *Frontiers in cellular neuroscience* **15**, 618658 (2021).

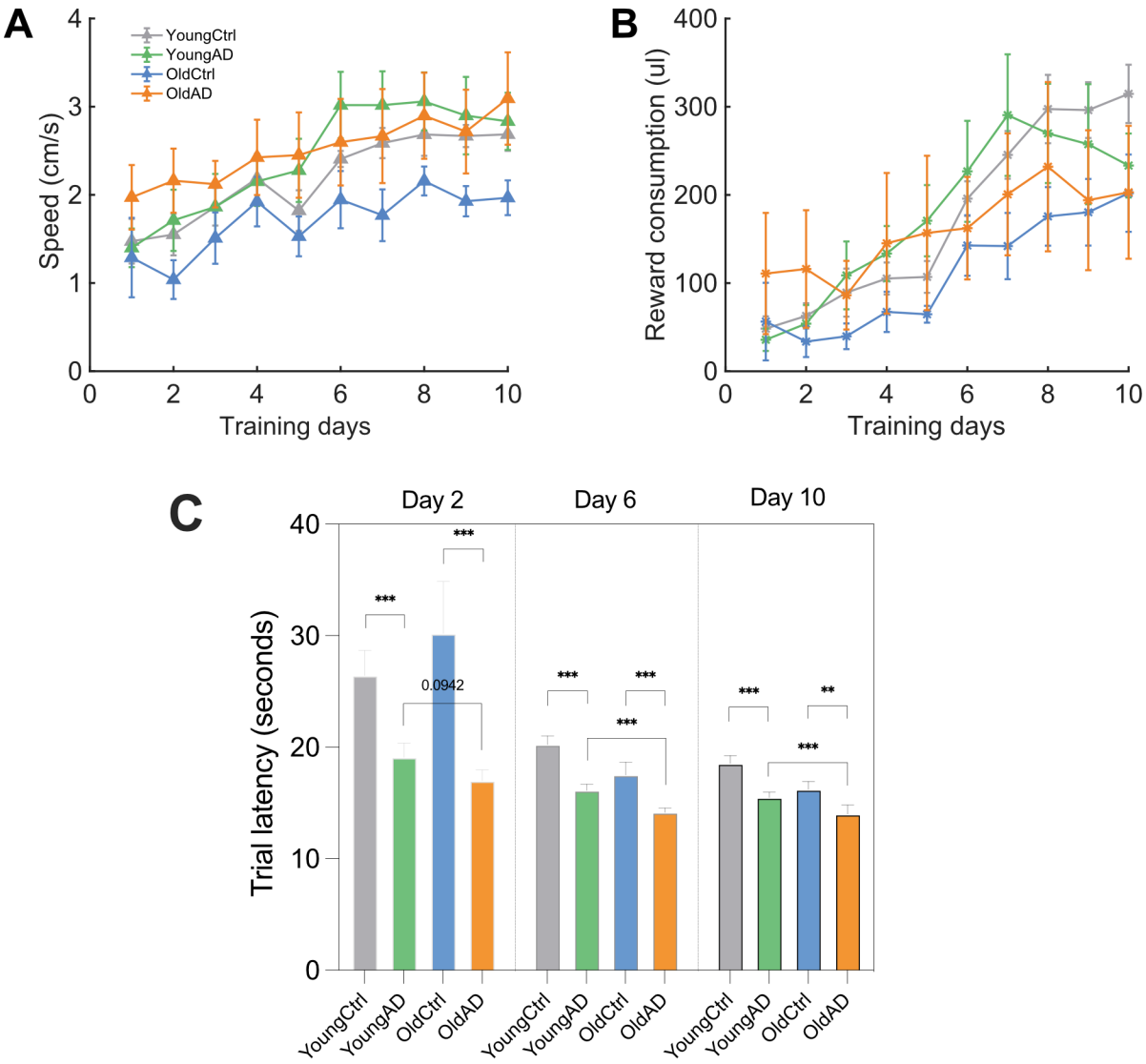

Supplementary Figure 1: Aged 5xFAD mice show behavioural hyperactivity

A. Average speed (cm/s) on each training day from all experimental groups. Age progressively enhanced locomotion in 5xFAD mice. AD effect ($F_{(1,330)}$ = 19.6, P <0.0001) and AD × Age effect ($F_{(1,330)}$ = 4.9, P = 0.027). YoungCtrl N=10, YoungAD N=8, OldCtrl N=6, OldAD N=7. Two-way ANOVA test.

B. Average reward consumption (μl) on each training day from all experimental groups. Age progressively reduced reward consumption in WT mice. AD effect ($F_{(1,330)}$ = 0.75, P=0.37) and Age effect ($F_{(1,330)}$ = 6.84, P = 0.009). Two-way ANOVA with post-hoc test. Old control mice showed reduced reward consumption compared to young control mice. YoungCtrl vs OldCtrl, P= 0.009. Data are shown as mean ± SEM.

C. Median with 95% CI of trial duration (seconds) in day 2, 6 and 10 training. The number of mice in each group: YoungCtrl N=10, YoungAD N=8, OldCtrl N=6, OldAD N=7. Mann-Whitney test was used. ** and *** indicate the significance levels with the respective P values of < 0.005 and < 0.0001.

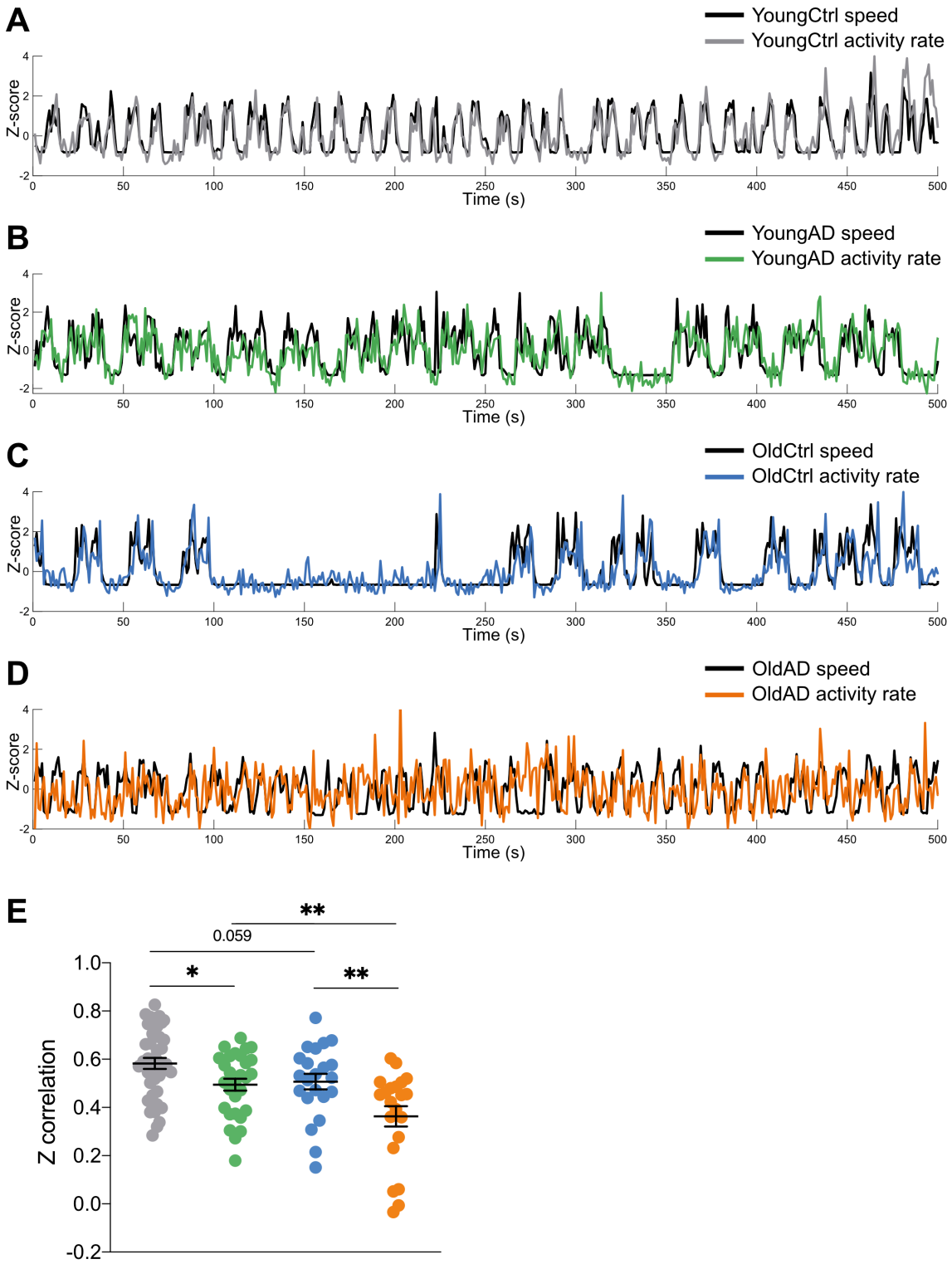
A
YoungCtrl speed
YoungCtrl activity rate
Z-score
Time (s)
B
YoungAD speed
YoungAD activity rate
Z-score
Time (s)
C
OldCtrl speed
OldCtrl activity rate
Z-score
Time (s)
D
OldAD speed
OldAD activity rate
Z-score
Time (s)
E
**
0.059
*
**
Z correlation

Supplementary Figure 2: Time coherence in speed and CA1 neural activity rate is impaired in 5xFAD mice.

A-D. Representative time series data, illustrating the Z-score of mouse locomotion speed (black) alongside the Z-score of CA1 neural calcium activity rates.

E. The Pearson's correlation coefficient between animals' Z-scored speed and population-average neural activity rate for the imaging field of view. YoungCtrl: 0.58±0.02, YoungAD:0.49±0.02, OldCtrl: 0.51±0.03, OldAD: 0.36±0.04. Data pooled from all imaging sessions in each animal group. Two-way ANOVA test with Tukey post hoc test. * and ** indicate the significance levels with the respective P values of < 0.05 and < 0.005.

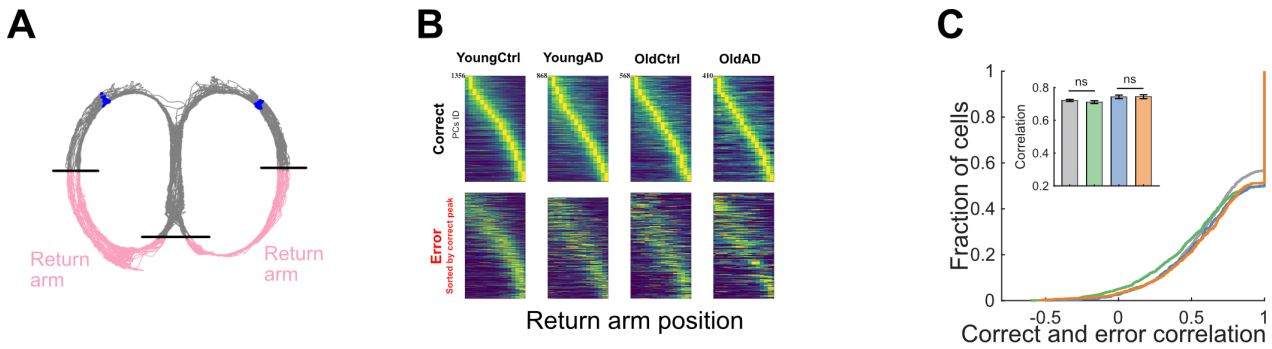

Supplementary Figure 3: The spatial correlation between correct and error trials in the return arm.

- **A.** Typical mouse trajectory in a continuous alternation task session. Choice-reward arm (pink), reward location (blue), and other arms (grey) are indicated.
- **B.** Normalized peak place cell activity along reward arm position. Top: correct trials, Bottom: error trials. Sorted by peak activity during correct trials.
- **C.** Cumulative plots with inset bar plots illustrate the spatial correlation of return-arm place cell activity between correct and error trials was normal in 5xFAD mice. Bar plots show data as mean ± s.e.m.. Two-way ANOVA test with Tukey post hoc test. ns. Indicates significance levels with *p* values > 0.05.

Fig	Data	Mean	SEM	Statistical test	n	Outcome measure	p value
Fig. 2F	YoungCtrl YoungAD OldCtrl OldAD	56.19 44.59 39.17 26.96	3.17 3.99 3.14 3.92	Scheirer-Ray-Hare test with Bonferroni post hoc test	41 29 24 21	Place cells proportion	Age effect: F(1,114)=21.76, p=0 AD effect: F(1,114)=10.28, p=0.0018 Age×AD effect: F(1,114)=0.01, p=0.93 YoungCtrl vs YoungAD: 0.047 OldCtrl vs OldAD: 0.028 YoungCtrl vs OldCtrl: 0.0003 YoungAD vs OldAD: 0.028
Fig. 2G	YoungCtrl YoungAD OldCtrl OldAD	3.8321 3.3232 3.1339 2.7853	0.0328 0.0343 0.0471 0.0423	Scheirer-Ray-Hare test with Bonferroni post hoc test	5363 2780 1608 1261	Place cells spatial information	Age effect: F(1,11011)=176.6, p=0 AD effect: F(1,11011)=84.9 p=0. Age×AD effect: F(1,11011)=2.9, p=0.08 YoungCtrl vs YoungAD: 2.73×10^{-24} OldCtrl vs OldAD: 6.19×10^{-5} YoungCtrl vs OldCtrl: 1.28×10^{-30} YoungAD vs OldAD: 2.97×10^{-13}
Fig. 3B	YoungCtrl YoungAD OldCtrl OldAD	0.8594 0.7958 0.8376 0.7895	0.0014 0.0021 0.0026 0.0028	Scheirer-Ray-Hare test with Bonferroni post hoc test	13223 7265 4234 3798	Place cells active trials ratio	Age effect: F(1,28516)=64, p=1.03×10^{-15} AD effect: F(1,28516)=807, p=1.49×10^{-177} Age×AD effect: F(1,28516)=4, p=0.046 YoungCtrl vs YoungAD: 2.58×10^{-133} OldCtrl vs OldAD: 3.64×10^{-44} YoungCtrl vs OldCtrl: 1.48×10^{-13} YoungAD vs OldAD: 0.002
Fig. 3D	YoungCtrl YoungAD OldCtrl OldAD	0.1100 0.0920 0.0917 0.0858	0.0008 0.0009 0.0013 0.0012	Scheirer-Ray-Hare test with Bonferroni post hoc test	13223 7265 4234 3798	Place cells trial-trial spatial correlation	Age effect: F(1,28516)=162, p=2.80×10^{-37} AD effect: F(1,28516)=161, p=6.69×10^{-37} Age×AD effect: F(1,28516)=35, p=3.92×10^{-9} YoungCtrl vs YoungAD: 1.65×10^{-43} OldCtrl vs OldAD: 0.0012 YoungCtrl vs OldCtrl: 6.10×10^{-40} YoungAD vs OldAD: 9.7×10^{-5}
Fig.4E(Early)	YoungCtrl YoungAD OldCtrl OldAD	0.598 0.413 0.3406 0.2596	0.0443 0.0937 0.0313 0.0555	Two-way ANOVA test with Tukey post hoc test	10 7 4 6	Stable place cells/PCs proportion	Age effect: F(1,25)=8.5, p=0.008 AD effect: F(1,25)=3.56, p=0.0724 Age×AD effect: F(1,25)=0.54, p=0.4683 YoungCtrl vs YoungAD: 0.2234 OldCtrl vs OldAD: 1 YoungCtrl vs OldCtrl: 0.1047 YoungAD vs OldAD: 0.8156 YoungCtrl vs OldAD: 0.0085
Fig.4E (Mid)	YoungCtrl YoungAD OldCtrl OldAD	0.5582 0.3469 0.2948 0.2493	0.0482 0.071 0.0254 0.0913	Two-way ANOVA test with Tukey post hoc test	10 7 4 6	Stable place cells/PCs proportion	Age effect: F(1,26)=6.69, p=0.0165 AD effect: F(1,26)=3.39, p=0.0787 Age×AD effect: F(1,26)=1.41, p=0.2472 YoungCtrl vs YoungAD: 0.1214 OldCtrl vs OldAD: 1 YoungCtrl vs OldCtrl: 0.0982 YoungAD vs OldAD: 1 YoungCtrl vs OldAD: 0.0121
Fig.4E(Final)	YoungCtrl YoungAD OldCtrl OldAD	0.5215 0.3652 0.4442 0.2273	0.0349 0.0581 0.0831 0.0744	Two-way ANOVA test with Tukey post hoc test	10 7 4 6	Stable place cells/PCs proportion	Age effect: F(1,26)=3.23, p=0.0856 AD effect: F(1,26)=9.7, p=0.0049 Age×AD effect: F(1,26)=0.26, p=0.6176 YoungCtrl vs YoungAD: 0.2541 OldCtrl vs OldAD: 0.1941 YoungCtrl vs OldCtrl: 1 YoungAD vs OldAD: 0.6385 YoungCtrl vs OldAD: 0.0048
Fig.4F	YoungCtrl YoungAD OldCtrl OldAD	0.3319 0.1917 0.1547 0.0815	0.0451 0.0592 0.0283 0.0378	Two-way ANOVA test with Tukey post hoc test	10 7 4 6	Stable place cells/all cells proportion	Age effect: F(1,26)=7.52, p=0.0116 AD effect: F(1,26)=4.15, p=0.0534 Age×AD effect: F(1,26)=0.41, p=0.5294 YoungCtrl vs YoungAD: 0.2267 OldCtrl vs OldAD: 1 YoungCtrl vs OldCtrl: 0.1774 YoungAD vs OldAD: 0.8306 YoungCtrl vs OldAD: 0.0062
Fig.4G	YoungCtrl YoungAD OldCtrl OldAD	0.4603 0.4886 0.4582 0.04682	0.0066 0.0078 0.0151 0.0118	Scheirer-Ray-Hare test	660 384 88 176	Session-to-session correlation	Age effect: F(1,1307)=0.92, p=0.337 AD effect: F(1,1307)=2.67, p=0.1023 Age×AD effect: F(1,1307)=0.6, p=0.4381
Fig.4H	YoungCtrl YoungAD OldCtrl OldAD	0.0193 0.4236 0.6417 0.7031	0.4347 0.4999 1.0339 0.7066	Scheirer-Ray-Hare test	1090 772 240 512	(Linearized) PF shift (cm)	Age effect: F(1,2610)=2.03, p=0.1544 AD effect: F(1,2610)=0.020, p=0.888 Age×AD effect: F(1,2610)=0.1170, p=0.7323
Fig.5C (correct)	YoungCtrl YoungAD OldCtrl OldAD	1.3921 1.0416 1.1852 1.0186	0.0174 0.0149 0.0229 0.0178	Two-way ANOVA test with Tukey post hoc test	3670 2609 1567 1285	reward PCs peak spatial tuning activity	Age effect: F(1,9130)=31.51, p=2.04×10^{-8} AD effect: F(1,9130)=159.45, p=3.00×10^{-36} Age×AD effect: F(1,9130)=20.15, p=7.25×10^{-6} YoungCtrl vs YoungAD: 3.77×10^{-9} OldCtrl vs OldAD: 5.11×10^{-6} YoungCtrl vs OldCtrl: 3.77×10^{-9} YoungAD vs OldAD: 0.876

Fig.5D(error)	YoungCtrl YoungAD OldCtrl OldAD	1.4694 1.1059 1.2092 0.9443	0.0231 0.0199 0.0351 0.0262	Two-way ANOVA test with Tukey post hoc test	3475 2455 1383 1165	reward PCs peak spatial tuning activity	Age effect: F(1,8477)=54.68, p=0 AD effect: F(1,8477)=121.38, p=0 Age×AD effect: F(1,8477)=3, p=0.0835 YoungCtrl vs YoungAD: 3.77×10^{-9} OldCtrl vs OldAD: 1.55×10^{-7} YoungCtrl vs OldCtrl: 3.81×10^{-9} YoungAD vs OldAD: 8.40×10^{-4}
Fig.5E	YoungCtrl YoungAD OldCtrl OldAD	1.1608 0.7938 0.8825 2.4888	0.1555 0.1532 0.1956 0.2115	Kruskal-Wallis test with Bonferroni post hoc test	1169 1188 664 669	reward cells peak activity apart from reward (cm)	Chi=42.79, $p=2.72\times10^{-9}$ YoungCtrl vs YoungAD: 1 OldCtrl vs OldAD: 2.43×10^{-6} YoungCtrl vs OldCtrl: 1 YoungAD vs OldAD: 1.32×10^{-7}
Fig.5G	YoungCtrl YoungAD OldCtrl OldAD	0.5001 0.3924 0.3624 0.3223	0.005 0.0063 0.0088 0.0099	Two-way ANOVA test with Tukey post hoc test	3054 2327 1329 1025	reward PCs correct and error spatial correlation	Age effect: F(1,7335)=184.95, $p=1.28\times10^{-41}$ AD effect: F(1,7335)=93.58, $p=5.29\times10^{-22}$ Age×AD effect: F(1,7335)=19.58, $p=9.78\times10^{-6}$ YoungCtrl vs YoungAD: 1.27×10^{-36} OldCtrl vs OldAD: 0.0102 YoungCtrl vs OldCtrl: 1.80×10^{-41} YoungAD vs OldAD: 7.21×10^{-9}
Fig.7A	YoungCtrl YoungAD OldCtrl OldAD	0.5332 0.4199 0.5041 0.4252	0.0094 0.0137 0.017 0.0201	Two-way ANOVA test with Tukey post hoc test	624 402 243 224	Splitting extent	Age effect: F(1,1491)=0.6, p=0.4 AD effect: F(1,1491)=42.96, p=0 Age×AD effect: F(1,1491)=1.43, p=0.23 YoungCtrl vs YoungAD:3.8×10^{-9} OldCtrl vs OldAD: 0.006 YoungCtrl vs OldCtrl: 0.46 YoungAD vs OldAD: 0.99
Fig.7B	YoungCtrl YoungAD OldCtrl OldAD	0.3732 0.3209 0.4157 0.2647	0.0086 0.012 0.0163 0.0157	Two-way ANOVA test with Tukey post hoc test	624 402 243 224	Splitting discriminability	Age effect: F(1,1491)=0.27, p=0.6 AD effect: F(1,1491)=60.7, p=0 Age×AD effect: F(1,1491)=14.31, p=0.0002 YoungCtrl vs YoungAD: 0.00003 OldCtrl vs OldAD: 0.004 YoungCtrl vs OldCtrl: 0.17 YoungAD vs OldAD: 0.16
Fig.7C	YoungCtrl YoungAD OldCtrl OldAD	0.1096 0.087 0.0804 0.0489	0.004 0.0057 0.0055 0.0047	Two-way ANOVA test with Tukey post hoc test	624 402 243 224	Splitting trial-trial reliability	Age effect: F(1,1491)=36.8, p=0 AD effect: F(1,1491)=23.67, p=0 Age×AD effect: F(1,1491)=0.65, p=0.42 YoungCtrl vs YoungAD: 0.002 OldCtrl vs OldAD: 3.8×10^{-9} YoungCtrl vs OldCtrl: 0.07 YoungAD vs OldAD: 0.019
Fig.7D	YoungCtrl YoungAD OldCtrl OldAD	0.0665 0.1099 0.0895 0.1359	0.005 0.0084 0.0091 0.0119	Two-way ANOVA test with Tukey post hoc test	624 402 243 224	first splitting occurrence	Age effect: F(1,1491)=8.54, p=0.004 AD effect: F(1,1491)=28.69, p=0 Age×AD effect: F(1,1491)=0.03, p=0.86 YoungCtrl vs YoungAD: 0.00003 OldCtrl vs OldAD: 0.004 YoungCtrl vs OldCtrl: 0.17 YoungAD vs OldAD: 0.16

Supplementary table 1. Statistical results